
Geomorphology and Watershed Management



Temporal and Spatial Distribution of Landslides in the Redwood Creek Basin, Northern California

M.A. Madej

Abstract

Mass movement processes are a dominant means of supplying sediment to mountainous rivers of north coastal California, but the episodic nature of landslides represents a challenge to interpreting patterns of slope instability. This study compares two major landslide events occurring in 1964–1975 and in 1997 in the Redwood Creek basin in north coastal California. In 1997, a moderate-intensity, long-duration storm with high antecedent precipitation triggered 317 landslides with areas greater than 400 m² in the 720-km² Redwood Creek basin. The intensity-duration threshold for landslide initiation in 1997 was consistent with previously published values. Aerial photographs (1:6,000 scale) taken a few months after the 1997 storm facilitated the mapping of shallow debris slides, debris flows, and bank failures. The magnitude and location of the 1997 landslides were compared to the distributions of landslides generated by larger floods in 1964, 1972, and 1975. The volume of landslide material produced by the 1997 storm was an order of magnitude less than that generated in the earlier period. During both periods, inner gorge hillslopes produced many landslides, but the relative contribution of tributary basins to overall landslide production differed. Slope stability models can help identify areas susceptible to failure. The 22 percent of the watershed area classified as moderately to highly unstable by the SHALSTAB slope stability model included locations that generated almost 90 percent of the landslide volume during the 1997 storm.

Keywords: landslides, rainfall intensity duration, slope stability model

Madej is a research geologist with the U.S. Geological Survey, Arcata, CA 95521. Email: mary_ann_madej@usgs.gov.

Introduction

Mass movement processes are a dominant means of supplying sediment to mountainous rivers of north coastal California, but the episodic nature of landslides represents a challenge to interpreting patterns of slope instability. Natural factors, including bedrock geology, topography, and vegetation, influence landslide occurrence. Many anthropogenic factors, such as logging and road construction, also affect slope stability (Swanston and Swanson 1976, Sidle and Wu 2001). These factors commonly do not come into play until a major storm occurs and high rainfall triggers landslide processes, including shallow debris slides and debris flows. It would be useful to know what type of rainfall conditions initiate landslides in this region and whether areas that exhibited landslide activity previously are susceptible to further mass movement in subsequent storms. Rainfall-triggering events were described by Caine (1980), who suggested a threshold of landslide initiation on the basis of a combination of intensity and duration for 73 rainfall events. More recently, Guzzetti et al. (2008) updated this threshold on the basis of 2,626 rainfall events. To date, landslide occurrence in north coastal California has not been evaluated in terms of these thresholds.

Landslide hazard assessment may use multivariate correlations between mapped landslides and landscape attributes or may employ a physics-based approach (Montgomery et al. 1998). The physical models of slope stability use information on topographic convergence and slope steepness to identify potentially unstable sites. One such model is SHALSTAB (Montgomery and Dietrich 1994), which has been used to assess the relation between forest clearing and shallow debris sliding in Oregon and Washington (Montgomery et al. 2000).

The objectives of this study are to compare the spatial distribution of landslides in the Redwood Creek basin during two periods of high landslide activity, to relate

the timing of landslide occurrence to precipitation patterns, and to assess the use of a slope stability model in predicting landslide occurrence.

Field Setting

Redwood Creek drains a 720-km² watershed in north coastal California and empties into the Pacific Ocean near Orick, CA. The basin is underlain primarily by Cretaceous and Late Jurassic metamorphic and sedimentary units of the Franciscan assemblage (Harden et al. 1982). Massive sandstones and interbedded sandstones and mudstones of the Coyote Creek and Lacks Creek units are on the east side of the watershed, whereas the west side is dominated by the Redwood Creek schist. The contrasting lithologies are separated by the highly sheared, slightly metamorphosed sandstone and mudstone of the Grogan Fault zone. Redwood Creek generally follows the trace of the fault, establishing a 100-km-long watershed with an average width of only 9 km. For about 50 km of its length the river flows through an inner gorge, where slopes that are adjacent to the stream channel are steeper than those farther upslope and are separated by a distinct break-in-slope (Kelsey 1988). Basin relief is 1,615 m and mean slope in the watershed is 25 percent. Mean annual rainfall in the watershed varies by location, ranging from about 2,500 mm at the headwaters to 1,520 mm near the mouth (Iwatsubo et al. 1975). Summers are dry, and almost all rainfall occurs between October and April. Snow is often present for several months at the highest elevations but is uncommon below 800 m.

Old-growth redwood (*Sequoia sempervirens*) and Douglas-fir (*Pseudotsuga menziesii*) originally dominated the downstream third of the Redwood Creek basin. Farther inland, Douglas-fir was the dominant conifer on the hillslopes, except for grasslands and oak woodlands on the drier ridges on the eastern divide. Intensive logging began in the watershed in the late 1940s, with most activity in the Douglas-fir forests of the middle and upper basin. Logging of redwoods accelerated in lower Redwood Creek in the early 1960s, and about 37 percent of the basin had been logged by the time of a large flood in 1964 (Best 1995). Most of the area was clearcut logged in large units and yarded using tractors, which resulted in extensive ground disturbance and a high density of roads. Stands of old-growth redwood remained in the lower basin, and in 1968 about 124 km² of the lower basin was acquired to form Redwood National Park (RNP). By 1978 about 80 percent of the original coniferous forest

had been logged. At that point, RNP boundaries were expanded to include an additional 150 km² of recently logged land that would be restored and managed as a protective buffer for the old-growth stands.

The Redwood Creek watershed has been subjected to a sequence of major floods since logging began. Since 1953, the U.S. Geological Survey (USGS) has operated a stream gauging station near the mouth of Redwood Creek at Orick, CA, where stream discharge and suspended sediment are measured. The 1964 flood attained the largest discharge on record (1,430 m³/s, a 50-year recurrence interval) and triggered the most landsliding (Harden 1995, Kelsey et al. 1995, Pitlick 1995). Additional floods of 1955, 1972, and 1975 all exceeded 1,390 m³/s. The 1997 flood was the largest since 1975 and peaked at 1,140 m³/s, representing a 10-year flow.

Surficial failures generated by the storms included debris slides and debris flows. Debris slides are rapid, shallow, dominantly translational slope failures along nearly planar surfaces, whereas debris flows are rapid failures along narrow, well defined tracks which show signs of flowing. In localized areas, Redwood Creek undercut adjacent hillslopes, resulting in large streambank failures. Earthflows, slow-moving complexes of slumping, flowing, and translational sliding that produce hummocky and lobate topography, are present in the Redwood Creek basin but were not quantified in the present study.

Methods

This study uses data on landslide distribution from several principal sources. Earlier studies of landslides in the Redwood Creek basin (Kelsey et al. 1995, Pitlick 1995) included extensive field measurements of landslide length, width, and depth on about 1,200 streamside landslides along the mainstem and in 16 of the largest tributaries. These studies provided the basis for comparison with more recent landsliding. Curry (2007) mapped the distribution of landslides generated by the January 1997 storm on 1:6,000 monochrome aerial photographs taken in June 1997, and the maps were updated for this study with further photographic examination. Landslide locations were transferred to orthophotos and then digitized. Landslide volumes were estimated from scar areas using a relation between area and volume constructed from previous field measurements of landslide dimensions in the basin (Kelsey et al. 1995, Pitlick 1995) and assuming the average hillslope gradient of 55 percent applies to

the scar site. Mean depths for debris flow tracks with areas greater than 3,000 m² were assumed to be 1.2 m on the basis of field observations. The Prairie Creek basin, a tributary basin near the mouth of Redwood Creek that is primarily covered with old-growth redwood forests, was not included in the earlier landslide studies so is not addressed in this update. The present comparison of landslides is restricted to landslides larger than 400 m² on the basis of a comparison of sizes of field-mapped landslides with the ability to detect them on 1:6,000 air photos.

Precipitation data for various time intervals for the 1997 storm are available from a tipping bucket gauge on the eastern divide of Redwood Creek at an elevation of 750 m. Several other nearby rain gauges were plagued with equipment problems, resulting in data gaps. Equivalent ridge-line data are not available for earlier storms, but storm totals near the mouth of Redwood Creek (station elevation of 50 m) for 1964 were compiled by Harden (1995).

The SHALSTAB slope stability model (Montgomery and Dietrich 1994) previously had been applied to the Redwood Creek basin on the basis of 10-m digital elevation models (DEMs) (Hare 2003). A stability rating, ranging from unconditionally stable to unconditionally unstable, was computed for each DEM cell on the basis of $\log(q/T)$, where T is the soil transmissivity and q is the effective precipitation (Montgomery and Dietrich 1994). To compare actual landslide locations with predicted unstable areas, the landslide maps were overlain onto a map of $\log(q/T)$ values. The stability of a landslide location was classified according to the least stable value of $\log(q/T)$ that was touched by the landslide scar, assuming that the least stable cell controlled the stability of the landslide.

Results

Following the 1997 storm, 317 landslides >400 m² in area were mapped in the Redwood Creek basin. Cumulatively these landslides mobilized 596,000 m³ of material, of which about 441,000 m³ was delivered to stream channels on the basis of air photo interpretation. Shallow debris slides ($n = 157$, median volume of 1,280 m³) accounted for about half the landslide features and 43 percent of the total landslide volume. Debris flows were slightly fewer in number ($n = 147$) but were somewhat larger (median volume of 1,870 m³) and accounted for 54 percent of the landslide volume. Only 13 streambank failures >400 m² in area

were identified (median volume of 1,060 m³). The volume of landslide material delivered to Redwood Creek and its tributaries during the 1997 storm was an order of magnitude less than the 4,000,000 m³ estimated to have been produced by storms between 1954 and 1978, of which most is likely to date from the 1964 storm (Kelsey et al. 1995).

In 1997, 20 percent of the landslides accounted for 56 percent of the total volume (Figure 1). The maximum size was 28,000 m³. Large landslides also dominated the size distribution in earlier periods, when 20 percent of the landslides contributed 72 percent of the volume and the largest landslide was 86,000 m³. The smallest 20 percent of the landslides only contributed 4 percent of the landslide volume in 1997 and 2 percent in the earlier period.

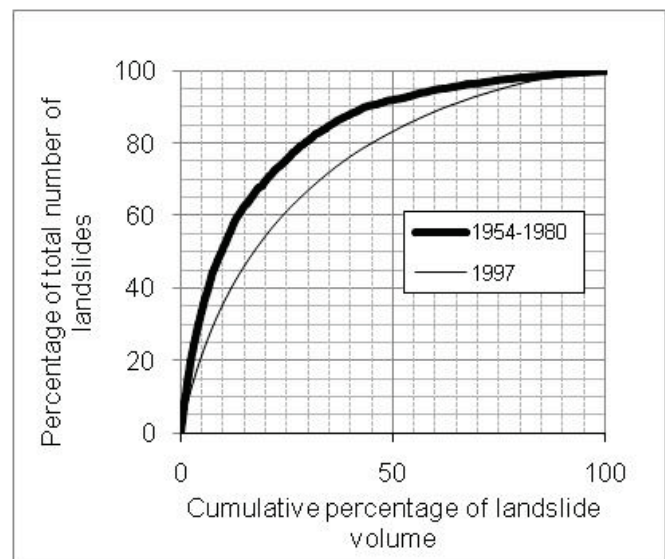


Figure 1. Cumulative volume-frequency relations for landslides in the Redwood Creek basin during two time periods.

The spatial distribution of landslide occurrence between the two time periods of 1954–1978 and 1997 is compared in Figure 2. In general, although the earlier time period produced an order of magnitude greater landslide volume, two inner gorge reaches along the mainstem of Redwood Creek identified as high landslide input areas in the earlier study (0–18 km, and 60–70 km from the headwaters) also had high landslide activity in 1997. In contrast, some tributary basins that had many active landslides in earlier periods were relatively inactive in 1997. Note that large tributary inputs are indicated by steep steps in the cumulative volume profile in Figure 2. For example, the reach between Copper Creek and Bridge Creek had high landslide activity in the earlier period but was relatively

quiescent in 1997. Windy, Minor, and Copper creeks were high sediment producers during the period of 1954–1978 but proportionately were not as great in 1997. The rates of timber harvest and road construction were lower in recent years, and most of the logging roads in the Copper Creek basin had been decommissioned in the mid 1980s, well before the 1997 storm. As a fraction of total landslide volume, Bridge and McArthur creek watersheds, where several large road-associated debris flows occurred, were relatively larger landslide producers in 1997 than in the earlier period.

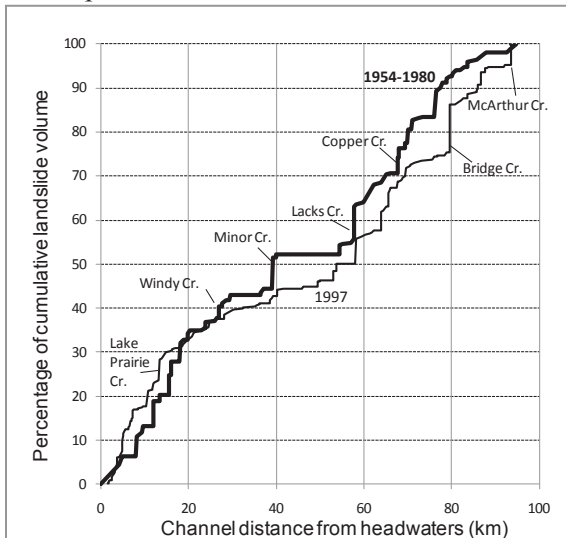


Figure 2. Comparison of volume of landslide material, cumulative over distance downstream along mainstem Redwood Creek, contributed for two time periods.

To assess whether the landslide-producing storms met the threshold rainfall values proposed by previous studies, data from Redwood Creek were compared to previously published relationships (Figure 3). For the 1- to 48-hour durations, rainfall in the Redwood Creek basin slightly exceeded the lower threshold defined by Caine (1980) and significantly exceeded the threshold for cool, Mediterranean climates defined by Guzzetti et al. (2008). Only the 15-minute rainfall duration did not have a corresponding intensity that exceeded the minimum threshold. The values for the 1964 storm also were consistent with the Caine relationship. The Guzzetti threshold for a cool, Mediterranean climate has a similar slope as Caine’s but predicts the likely occurrence of shallow failures at lower rainfall intensities. Caine’s threshold was established for catastrophic slope failures, whereas the Guzzetti threshold may represent a minimum boundary for smaller landslides. In the case of the Redwood Creek watershed, we have observed occasional failures during years with rainfall intensities or durations less than

Caine’s threshold, but widespread landsliding did not occur until Caine’s threshold was exceeded.

Areas predicted to be unstable through the SHALSTAB slope stability model were compared to the volume of landslide material mobilized during the 1997 storm (Table 1). High, moderately high, and moderate potential for instability are represented by areas where $\log(q/T)$ is less than or equal to -3.1, -2.8, and -2.5, respectively (Montgomery et al. 1998). These stability classes accounted for 22 percent of the watershed area and included 85 percent of the number of sites that failed and 87 percent of the volume of material mobilized by landslides during the 1997 storm.

Discussion

A few large landslides account for the bulk of hillslope material eroded in widespread landsliding events. In the earlier period, massive inner gorge debris slides as large as 86,000 m³ stripped the hillslopes up to the break-in-slope. Although the inner gorge also produced many moderately large debris slides in 1997, the largest landslides at that time were debris flows originating from road fill failures on unpaved forest roads. It is possible that the earlier events removed the most unstable material in the inner gorge so that the supply of weathered colluvium available to fail in subsequent storms was diminished. The present focus of RNP and other basin landowners on decommissioning abandoned roads may decrease the number of road failures in future storms, but this erosion control work has not yet been “tested” by storms of the size seen in 1964, 1972, and 1975.

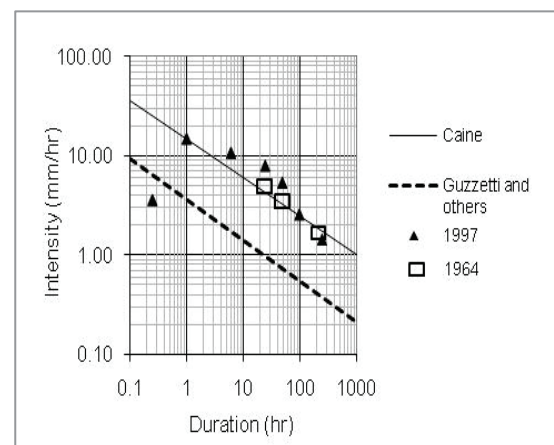


Figure 3. Rainfall intensity-duration for Redwood Creek storms and from other areas.

Table 1. Distribution of landslides and landslide scar volume by stability classes defined by the SHALSTAB slope stability model.

Stability class	Value range, $\log_{10}(q/T)$	Percent of watershed area ¹	Percent of slides	Percent of slide volume
Stable or low instability	> -2.2	71.2	9.3	8.7
Moderately low	-2.5 to -2.2	6.7	5.6	4.2
Moderate	-2.8 to -2.5	10.7	17.8	28.6
Moderately high	-3.1 to -2.8	6.4	21.5	19.9
High instability	< -3.1	4.8	45.8	38.5

¹Redwood Creek watershed, excluding Prairie Creek.

The initiation of widespread landsliding in the Redwood Creek basin seems to coincide with the intensity-duration threshold of initiation proposed by Caine (1980). The values of rainfall intensity-duration for the 1964 storm measured at an elevation of 50 m were less than those for the 1997 storm, measured at 630 m. It is very likely that the 1964 values were much higher at upper elevations owing to orographic effects but no high elevation rain gauges were present in the Redwood Creek basin at that time. In recent years more automated weather stations have been installed in the basin, which will help assess rainfall trends in future storms. Other factors in landslide initiation, such as land use and antecedent precipitation, probably also play roles. The 60-day antecedent precipitation index associated with the beginning of the 1997 storm, at 136 mm, was the fifth highest of the last seven flood-producing storms, previously analyzed by Harden (1995). Future research will examine the relationships among landslide occurrence, bedrock geology, timber harvest, and roads.

The slope stability model SHALSTAB performed well in identifying susceptible terrain producing large volume landslides in the Redwood Creek watershed. SHALSTAB was designed to model the susceptibility of terrain to shallow debris slides (Montgomery and Dietrich 1994). In the Redwood Creek basin, the model was able to account for 75 percent and 90 percent of the volume of shallow debris slides by classifying the most unstable 10 percent and 20 percent of the basin, respectively, which is similar to results obtained from other northern California watersheds (Dietrich et al. 2001). Because the 10-m DEMs underestimate slope steepness at the bottom of narrow, V-shaped valleys, the SHALSTAB results are conservative. Although not designed to predict debris flow locations, the model also accounted for debris flow volumes with accuracies similar to those for shallow debris slides. Failures from both roads and harvest areas are more likely in steep, convergent areas, which SHALSTAB was able to

detect from 10-m DEMs. Failures can, of course, also occur on slopes classified as stable or moderately stable if roads, landings, or timber harvest alter the hydrologic regime or mass balance of materials at a site. SHALSTAB can be used as a tool by land managers in timber harvest plan reviews or other planning activities to highlight areas of potential slope instability, and these areas can then be targeted for more detailed field investigations.

Conclusion

A large storm in January 1997 initiated 317 landslides in the Redwood Creek basin in north coastal California. In comparison to previous large storms, the 1997 event produced an order of magnitude less landslide volume. A few large landslides accounted for the bulk of the sediment volume, as 20 percent of the landslides produced 56 percent of the total landslide volume. Inner gorge slopes had a large number of landslides in earlier storms, and this pattern also held in the 1997 storm. Nevertheless, the largest landslides in 1997 were debris flows originating on forest roads. The rainfall intensity-duration threshold proposed by Caine (1980) held true for landslide initiation in 1997. The slope stability model, SHALSTAB, also performed well in predicting locations of landslide occurrence. The 22 percent of the watershed area classified as moderately to highly unstable by the model included locations generating almost 90 percent of the landslide volume during the 1997 storm.

Acknowledgments

Leslie Reid provided many insights during this project and suggested more avenues to explore. Greg Bundros and Kevin Andras verified landslides on the air photos and mapped the inner gorge as a GIS coverage. Daryl van Dyke helped me with the GIS portion of the SHALSTAB analysis. Tera Curry devoted many hours in the early stages of this project poring over air photos

and mapping landslides features. Andre Lehre and Greg Bundros made several useful suggestions to improve the manuscript.

References

- Best, D. 1995. History of timber harvest in the Redwood Creek Basin, northwestern California. In K.M. Nolan, H.M. Kelsey, and D.C. Marron, eds. *Geomorphic processes and aquatic habitat in the Redwood Creek Basin, northwestern California*, pp. C1–C7. U.S. Geological Survey Professional Paper 1454-C.
- Caine, N. 1980. The rainfall intensity-duration control of shallow landslides and debris flows. *Geografiska Annaler* 62(1–2):23–27.
- Curry, T.L. 2007. A landslide study in the Redwood Creek basin, northwestern California: Effects of the 1997 storm. M.S. thesis. Humboldt State University, Arcata, CA.
- Dietrich, W.E., D. Bellugi, and R. Real de Asua. 2001. Validation of the Shallow Landslide Model, SHALSTAB, for Forest Management. In M.S. Wigmosta and S.J. Burges, eds. *Land Use and Watersheds: Human Influence on Hydrology and Geomorphology in Urban and Forest Areas*, pp. 195–227. American Geophysical Union, Washington D.C.
- Guzzetti, F., S. Peruccacci, M. Rossi, and C.P. Stark. 2008. The rainfall intensity-duration control of shallow landslides and debris flows: An update. *Landslides* 5:3–17.
- Harden, D.R. 1995. A comparison of flood-producing storms and their impacts in northwestern California. In K.M. Nolan, H.M. Kelsey, and D.C. Marron, eds. *Geomorphic processes and aquatic habitat in the Redwood Creek Basin, northwestern California*, pp. D1–D9. U.S. Geological Survey Professional Paper 1454-D.
- Harden, D.R., H.M. Kelsey, S.D. Morrison, and T.A. Stephens. 1982. Geologic map of the Redwood Creek drainage basin, Humboldt County, California. U.S. 1:62,500. Geological Survey Open-File Report 81-496, scale
- Hare, V. 2003. Evaluation of a geographic information system model of shallow landsliding in Redwood Creek, California. M.S. thesis. Humboldt State University, Arcata, CA.
- Iwatsubo, R.T., K.M. Nolan, D.R. Harden, G.D. Glysson, and R.J. Janda. 1975. Redwood National Park studies, data release 1: Redwood Creek, Humboldt County, California, September 1, 1973–April 10, 1974. U. S. Geological Survey Open-file Report 76-678.
- Kelsey, H.M. 1988. Formation of inner gorges. *Catena* 15:433–458.
- Kelsey, H.M., M. Coghlan, J. Pitlick, and D. Best, 1995. Geomorphic analysis of streamside landslides in the Redwood Creek Basin, northern California. In K.M. Nolan, H.M. Kelsey, and D.C. Marron, eds. *Geomorphic processes and aquatic habitat in the Redwood Creek Basin, northwestern California*, J1–J12. U.S. Geological Survey Professional Paper 1454-J.
- Montgomery, D.R., K.M. Schmidt, H.M. Greenberg, and W.E. Dietrich. 2000. Forest clearing and regional landsliding. *Geology* 28(4):311–314.
- Montgomery, D.R., K. Sullivan, and H.M. Greenberg. 1998. Regional test of a model for shallow landsliding. *Hydrological Processes* 12: 943–955.
- Montgomery, D.R., and W.E. Dietrich. 1994. A physically based model for topographic control on shallow landslides. *Water Resources Research* 30: 1153–1171.
- Pitlick, J. 1995. Sediment routing in tributaries of the Redwood Creek basin, Northwestern California. In K.M. Nolan, H.M. Kelsey, and D.C. Marron, eds. *Geomorphic processes and aquatic habitat in the Redwood Creek Basin, northwestern California*, K1–K10. U.S. Geological Survey Professional Paper 1454-K.
- Sidele, R.C., and W. Wu. 2001. Evaluation of the Temporal and Spatial Impacts of Timber Harvesting on Landslide Occurrence. In M.S. Wigmosta and S.J. Burges, eds. *Land Use and Watersheds: Human Influence on Hydrology and Geomorphology in Urban and Forest Areas*, pp. 179–193. American Geophysical Union, Washington D.C.
- Swanston, D.N., and F.J. Swanson. 1976. Timber Harvesting, Mass Erosion, and Steepland Forest Geomorphology in the Pacific Northwest. In D.R. Coates, ed. *Geomorphology and Engineering*, pp. 199–221. Dowden, Hutchinson and Ross, Stroudsburg, PA.

Holocene Extraordinary Floods and the Social Impacts in the Weihe River Basin, China

Chunchang Huang, Jiangli Pang

Abstract

Holocene Palaeoflood slackwater deposits (SWD) were often found inserted in the loess-soil stratigraphy along the Weihe River valley near Xi'an in the middle Yellow River basin. These compacted silt or clayey silt beds were deposited from the suspended sediment load in the floodwater. They have recorded the extraordinary palaeoflood events during the Holocene. Typical SWD beds were identified at four sites during field investigations in the last three years. The SWD beds have recorded large Holocene floods that occurred between 3,200 and 3,000 years before present (B.P.) when the mid-Holocene Climatic Optimum was coming to a close. Using the end point of the SWD as the minimum flood stage, the minimum flood peak discharges were estimated to between 22,560 and 25,960 m³/s by using slope-area methods. The magnitude of these floods is 4.5–5.0 times the largest gauged flood (5,030 m³/s) that has ever occurred. The episode at about 3,000 B.P. in Chinese history is known as a most disastrous time because of the droughts, harvest failure, and great famine in connection with a monsoonal climatic shift, and also the marked social change, i.e. the replacement of the Shang dynasty by the Zhou dynasty. The frequently occurring natural hazards, including floods and droughts, may have destroyed the agricultural economy of the Shang dynasty and resulted in the collapse of the Shang dynasty in the Yellow River basin. These results are very important in understanding the social effect of hydroclimatic change in the semiarid to subhumid regions.

Huang and Pang are professors with the Department of Geography, Shaanxi Normal University, Xi'an, Shaanxi 710062, P. R. China. Email: cchuang@snnu.edu.cn, jlpan@snnu.edu.cn.

Paleochannels as Reservoirs for Watershed Management

R.P. Gupta, S. Kumar, R.K. Samadder

Abstract

Conservation of water needs suitable storage and management strategies. Surface storage through large dams has been a conventional method of water conservation, but it has its own well-known problems of land submergence, displacement of population, loss of agricultural land, etc. By integrating satellite sensor data, dedicated drilling borehole data, and field soil characteristics, etc., we have located three major paleochannels of the Ganges river in the Gangetic Plains and have studied their aquifer geometry and hydrogeologic characteristics. The three mapped paleochannels of the Ganges river cover an area of about 396 km² and would have a cumulative water storage capacity of approximately 4.65 billion cubic meters (idealized). Hydrogeologically, the aquifer is well interconnected with the adjacent alluvial aquifers. Monitoring of groundwater levels for two successive years (2006 and 2007) indicates that aquifers in alluvial plains are also recharged through paleochannels. Thus, it is inferred that such paleochannels can play a very important role in storage of water, artificial recharge of adjacent aquifers, and overall watershed management.

Keywords: Paleochannels, Gangetic Plains, hydrogeological characteristics, watershed management

Introduction

The Ganges is a major transboundary river of the Indian subcontinent, covering parts of four countries—India, Nepal, Tibet, and Bangladesh. It has a highly variable seasonal flow as its hydrologic cycle is governed by the South-West Monsoon. The average ratio of dry season to monsoon discharge is considered

to be 1:6. Though the average annual rainfall in the basin is >1,100 mm, it is largely confined to the monsoonal period (15 June–15 September), so severe water scarcity conditions often occur during the summer months (April–June). The water scarcity crisis is increasing in view of increased water demand for industrialization, intensive agriculture, and rising living standards.

A key issue lies, therefore, in water resource management through storage of a major part of the monsoonal flow, which now drains almost unabated into the ocean, and its beneficial use later during the lean period.

Surface storage through large dams has been a conventional method of water conservation, but it has its own well-known problems of land submergence, displacement of population, loss of agricultural land, etc. For example, the Tehri dam, one of the largest dams built on the Ganges river in the Himalayas, has a storage volume of 3.54 billion cubic meters (BCM) but has an areal submergence of 42 km² (at FRL) and population displacement of about 100,000 from nearly 100 villages.

Because of the steep slopes in the mountainous region and the topographically flat nature of the Gangetic Plains, surface sites for water storage are scarce and expensive and are laced with various issues and problems. On the other hand, there exist great possibilities for underground storage, which should be relatively inexpensive. In a classic paper (published in *Science*), Revelle and Lakshminarayana (1975) articulated the conjunctive use of ground and surface water in the Ganges basin. They suggested ways to increase infiltration along the piedmont zones and parts of the upper Ganges river system into the water table during the monsoon season, followed by abstracting groundwater from the aquifers during the dry period. This process could be operated cyclically like a machine.

Gupta is a professor with the Department of Earth Sciences, Indian Institute of Technology Roorkee, Roorkee-247667, India. Email: rpgupta.iitr@gmail.com. Kumar is a scientist with the National Institute of Hydrology, Roorkee-247667, India. Samadder is a geologist with the West Bengal State Water Resources Department, Kolkatta.

We would like to take the argument further in this paper. By integrating satellite sensor data, dedicated drilling borehole data, and field soil characteristics, etc., we have located three major paleochannels of the Ganges river in the Gangetic Plains and have studied their hydrogeologic characteristics. We believe that these paleochannels, and similar ones elsewhere, can play a very important role in water storage as well as in artificial recharge of adjacent aquifers.

Study Area and Methodology Overview

The area of study falls between longitudes 77°30'E to 78°10'E and latitudes 29°10'N to 29°50'N and lies in the districts of Saharanpur and Muzaffarnagar of Uttar Pradesh, India (Figure 1). The Indo-Gangetic Plains are almost devoid of any significant relief features. Geologically, the Pleistocene to Recent alluvial deposits cover the area. Morphologically, four major landforms—piedmont zone, plains associated with river, interfluvies, and paleochannels—have been recognised in the area (Kumar et al. 1996).

The data used in this study can be broadly categorized into three main groups: (a) remote sensing data, (b) ancillary data, and (c) field data. Remote sensing data from the Indian Remote Sensing (IRS) satellite mission (www.nrsc.gov.in) has been used. The IRS-LISS-II sensor image data in multispectral (green, 0.52–0.59 μm ; red, 0.62–0.69 μm ; near-infrared, 0.76–0.89 μm) bands have been geometrically registered, rectified for atmospheric haze effects, and edge-sharpened (Laplacian isotropic filter) for interactive interpretation.

Toposheets from Survey of India have been used to generate the base map. Soil map and hydrogeological data (such as specific yield, storage coefficient, etc.) of the aquifer have also been extracted from various existing maps, reports, and literature. In addition, extensive dedicated field work was carried out during July 2005–July 2007. Mention must be made of dedicated drilling operations carried out at selected 17 locations to varying depths of up to 60 m to collect subsurface lithologic data. Sites for drilling have been selected systematically within the paleochannels and on either side on the adjacent alluvial plains. Existing well log data from 70 vertical boreholes in the study area also have been collected, tabulated, and digitized. Software used in the study includes ERDAS Imagine-8.7, ILWIS-3.3, ARCVIEW-3.2, and ROCKWORKS-2006. The entire study has been carried out in the GIS environment.

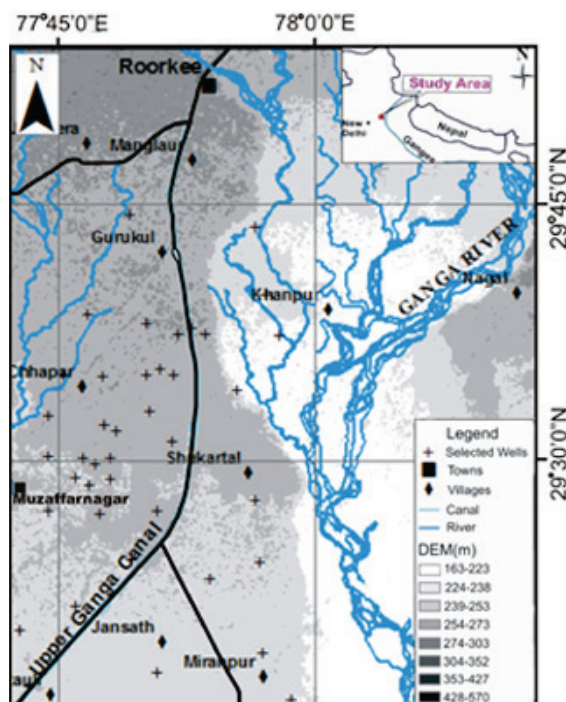


Figure 1. Location map of the study area over the digital elevation model.

Paleochannel Mapping

Owing to its synoptic view and map-like format, the satellite remote sensing imagery is a viable source for gathering quality regional data on landforms and land use/landcover (LULC) (Gupta 2003, Lillesand et al. 2007). In this area, five LULC classes have been identified: agricultural plains, paleochannel, water body, built-up area, and marshy land (Figure 2). The landcover types are closely related to the landform units (for details, see Samadder et al. 2011).

Integrating information from color infrared (CIR) composites, LULC map, field observations, and litholog data, paleochannels have been traced and mapped. Three major paleochannels exhibiting a broadly successive shifting and meandering pattern have been deciphered (Figure 2). All the paleochannels are quite wide (4–6 km), suggesting their formation by a large river. Litholog data indicates that the river paleochannel deposits are significantly different from the vast alluvial deposits in soil characteristics (particle size distribution, see below). The paleochannels are composed of coarse sand with pebbles, boulder, cobbles, etc., and appear genetically related to the well-developed regionally extensive historic river system. Low surface moisture and rather sparse vegetation on the paleochannels indicate highly permeable, porous, coarse grained materials with high infiltration rates.

Paleochannel Aquifer Geometry

Study of aquifer geometry is extremely important as it provides insight on aquifer areal extent, thickness, volume, aquifer boundaries, and interconnectivity between adjacent aquifers. This information has implications in water storage, lateral groundwater movement, and artificial groundwater recharge. Constructions of a subsurface lithological cross-section and aquifer geometry have been made by aggregating and synthesizing all the information, such as the base map, the CIR composite image, the paleochannel map, well location, and well log and elevation data. During the construction of a lithological cross-section and interpretation of aquifer geometry, it was observed that the aquifers also exhibit vertical displacements along normal faults at places (Samadder et al. 2007).

Hydrogeological Characteristics

Soil texture

Twenty surface soil samples collected from different sites located on both the paleochannels and alluvial plains were analyzed to determine soil texture. It is found that that the paleochannels comprise dominantly the sandy loam type of soil; on the other hand, the alluvial plains are characterised by a relatively finer silty loam type of soil.

Hydraulic conductivity

Hydraulic conductivity was estimated to ascertain the relative hydraulic properties of the paleochannels and the adjacent alluvial plains. A total of 82 soil samples

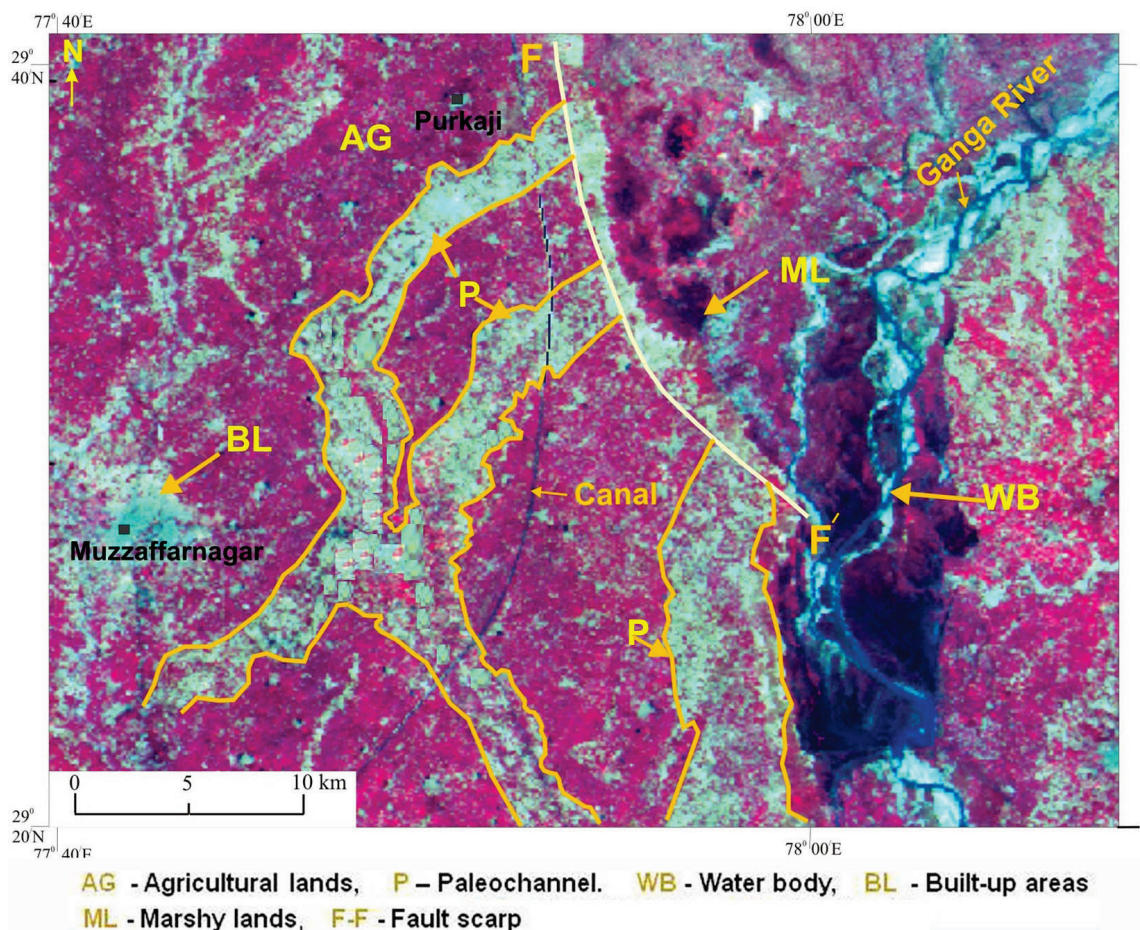


Figure 2. Color infra-red (CIR) composite generated from IRS-LISS-II satellite sensor data. Near-infrared band coded in red color; red band coded in green color, green band coded in blue color. Note the prominent paleochannels marked *P*.

were collected from different depths of wells. Bulk hydraulic conductivity was estimated for each sample from the grading curve method of Hazen approximation using D_{10} values (Hazen, 1911). The estimated bulk hydraulic conductivity for samples at different depths is found to range from 30 to 75.3 m/day for the paleochannel samples and from 13.5 to 22.3 m/day for the alluvial plains. These values are broadly corroborated by pumping test data where the values are found to range from 10 to 48 m/day in and around the area (Pandey et al. 1963).

Rate of natural groundwater recharge

Estimation of the natural rate of groundwater recharge (i.e., infiltration) is very important for assessing storage and artificial groundwater recharge. This can be done by measuring soil moisture movement in the unsaturated zone. The technique of estimation of recharge rate by using artificial tritium as a tracer (Zimmerman et al. 1967, Athavale and Rangarajan 2000) has been applied in this study area. The major source of recharge to groundwater in the study area is precipitation, about 85 percent of which occurs during the monsoon period (15 June–15 September). Field experiments have been performed at fourteen sites—eight within the paleochannel and six on the adjacent

alluvial plains—for natural recharge estimation. Tritium was injected at 70-cm depth (so that it is below the normal root zone) immediately before the monsoon period (June 2006). The soil samples were collected just before injection (June 2006) and after the monsoon (October 2006) and analyzed, as per the standard procedure (Samaddar et al. 2011). The results indicate a higher rate of recharge in the paleochannels (17.0–28.7 percent) as compared to the alluvial plains (6.3–11.0 percent).

Groundwater flow

A groundwater table map has been generated to establish the groundwater flow direction within the area. For this purpose, the depth to groundwater levels have been monitored in 37 observation wells (12 in the paleochannel aquifers and 25 in the adjacent alluvium plains) over a period of 2 years (2006 and 2007) both before and after the monsoon period. The computed groundwater elevation data was used to generate groundwater table contour maps and flow vector maps (Figure 3). The figure indicates that groundwater flows away from the paleochannel both before and after the monsoon period. The typical contour pattern (convex downwards) in the paleochannel aquifer is interpreted to be due to high porosity and permeability and its higher vertical hydraulic conductivity, further suggesting that groundwater recharge through paleochannels could lead to a gradual recharge of the adjacent alluvial plains.

Potential of Paleochannels for Acting as Reservoirs

The above results show that the paleochannels of the Ganges in this area possess an average width of almost 4–6 km and are quite extensive, running for a strike length of about 60–80 km. The paleochannel aquifer is unconfined and is mainly composed of coarse sandy material along with boulder and pebble beds and extends to a depth of about 65–70 m. The three mapped paleochannels of the Ganges river cover an area of about 396 km² on the surface and are computed to have a cumulative water storage capacity of approximately 4.65 BCM (idealized). The value of hydraulic conductivity ranges from 30 to 75 m/day in the paleochannel and from 13.5 to 22.3 m/day in the adjacent alluvial aquifers. The natural groundwater recharge rate due to precipitation is found to be 18.9–28.7 percent in the paleochannel area and 6.3–8.9 percent in the in the alluvial plains.

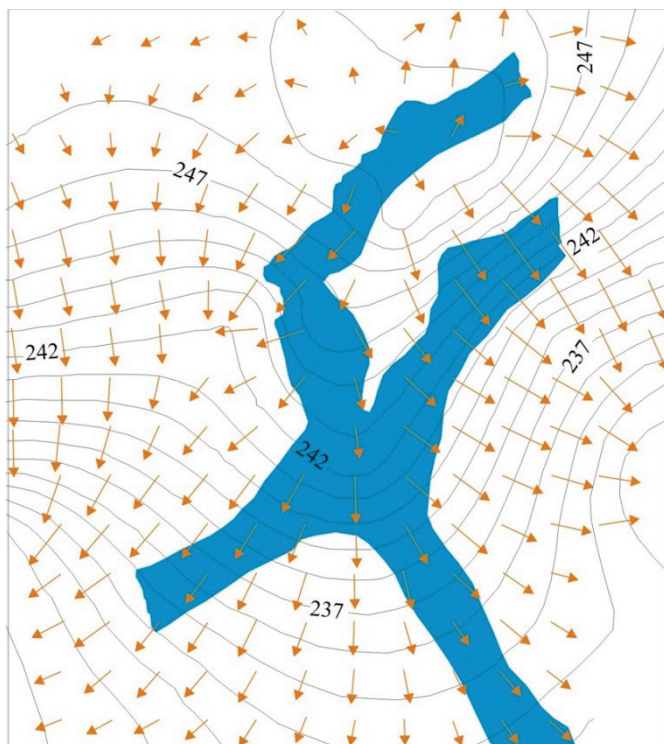


Figure 3. Typical groundwater level contours and flow direction map. Note that the paleochannels (blue) are recharging the aquifers.

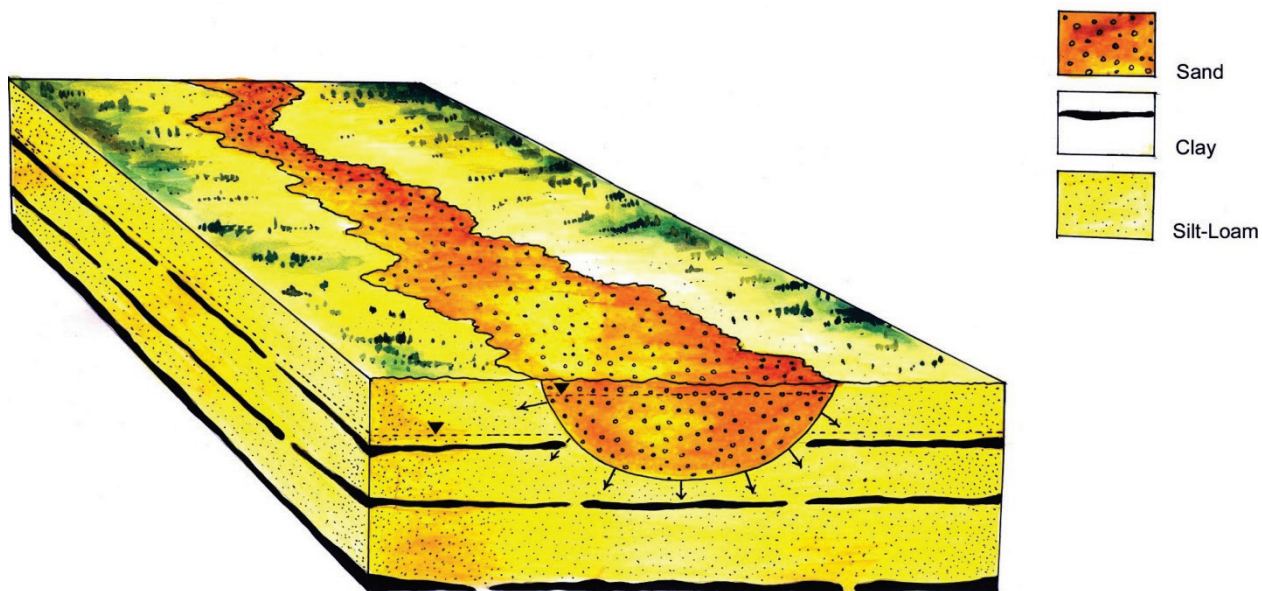


Figure 4. Schematic showing a paleochannel as a subsurface reservoir and source of continuous gradual recharge of groundwater.

It is observed that the paleochannel aquifer is well interconnected with the adjacent alluvial aquifers. Monitoring of groundwater levels for two successive years (2006 and 2007) indicates that the paleochannels also recharge the aquifers in the alluvial plains. Therefore, if paleochannel aquifers were used for storage of water and artificial recharge, water from the paleochannels would keep continuously flowing into the adjacent alluvial aquifers, making the paleochannels an almost infinite source of slow and gradual recharge (Figure 4).

In the area adjacent to the paleochannels, an average decline in the water table of about 0.24 m/year has been observed over a 10-year period. To arrest this decline, it is estimated that an annual recharge of about 30 MCM water is required per 1,000 km² of alluvial aquifer area (assuming specific field = 0.15), which can be easily accomplished by recharging through the paleochannel aquifers.

Thus, it is inferred that paleochannels of such hydrogeological characteristics and setting can play a very important role in water storage as well as in artificial recharge of adjacent aquifers. Apart from the Ganges and Indus Plains in India, the methodology can be applied for identification of similar suitable paleochannels in the alluvial tracts of the world, such as the Hwang Ho Plains in Northern China, the Po-Lombardy Plains of Italy, the Nile Plains of Egypt, and other areas.

Acknowledgments

The authors wish to thank Dr. B. Kumar and Mr. S.K. Verma, National Institute of Hydrology, Roorkee, for technical help in isotopic studies. The financial assistance from the Ministry of Water Resources, Government of India, New Delhi, is duly acknowledged. The authors appreciate the review comments of B.B.S. Singhal and G.J.Chakrapani.

References

- Athavale, R.N., and R. Rangarajan. 2000. Annual replenishable groundwater potential of India: An estimate based on injected tritium studies. *Journal of Hydrology* 234:38–53.
- Gupta, R.P. 2003. *Remote Sensing Geology* (2nd ed.). Springer-Verlag, Berlin-Heidelberg, Germany, 655 p.
- Hazen, A. 1911. Discussion: Dams on sand foundations. *Transactions of the American Society of Civil Engineers* 73:199-203.
- Kumar, S., B. Parkash, M.L. Manchanda, and A.K. Singhvi. 1996. Holocene Landform and Soil Evolution of the Western Gangetic Plains: Implications of Neotectonics and Climate. In K.H. Pfeffer, ed. *Tropical/Subtropical Geomorphology*, pp. 283–312. *Zeitschrift fur Geomorphologie, Supplementbande* 103.

Lillesand, T.M., R.W. Kiefer, and J. Chipman. 2007. Remote Sensing and Image Interpretation (6th ed.). John Wiley and Sons, New York, 804 p.

Pandey, M.P., K.V. Raghava Rao, and T.S. Raju. 1963. Groundwater resources of Tarai-Bhabar belts and intermontane doon valley of western Uttar Pradesh. Government of India, Ministry of Food and Agriculture, Exploratory Tubewells Organization, Bulletin series A no. 1.

Revelle, R., and V. Lakshminarayana. 1975. The Ganges water machine. *Science* 188:611–616.

Samadder, R.K., S. Kumar, and R.P. Gupta. 2007. Conjunctive use of well-log and remote sensing data for interpreting shallow aquifer geometry in Ganges Plains. *Journal of the Geological Society of India* 69:925–932.

Samadder, R.K., S. Kumar, and R.P. Gupta. 2011. Paleochannels and their potential for artificial groundwater recharge in the western Ganga plains. *Journal of Hydrology* 400:154–164.

Zimmerman, U., K.O. Munnich, and W. Roether. 1967. Downward Movement of Soil Moisture Traced by Means of Hydrogen Isotopes. In E.S. Glenn, ed. *Isotope Techniques in the Hydrologic Cycle*, pp. 28–36. American Geophysical Union, Geophysical Monograph 11.

The Effectiveness of Aerial Hydromulch as an Erosion Control Treatment in Burned Chaparral Watersheds, Southern California

Peter M. Wohlgemuth, Jan L. Beyers, Peter R. Robichaud

Abstract

High severity wildfire can make watersheds susceptible to accelerated erosion, which impedes resource recovery and threatens life, property, and infrastructure in downstream human communities. Land managers often use mitigation measures on the burned hillside slopes to reduce postfire sediment fluxes. Hydromulch, a slurry of paper or wood fiber that dries to a permeable crust, is a relatively new erosion control treatment. Delivered by helicopter, aerial hydromulch has not been rigorously field tested in wildland settings. Concerns have been raised over its ability to reduce watershed erosion along with its potential for negative effects on postfire ecosystem recovery. Since 2007 we have compared sediment fluxes and vegetation regrowth on plots treated with aerial hydromulch versus untreated controls for three wildfires in southern California. The study plots were all on steep slopes with coarse-textured soils that had been previously covered with mixed chaparral. Sediment production was measured with barrier fences that trapped the eroded sediment. Surface cover was repeatedly measured on meter-square quadrats. The aerial hydromulch treatment did reduce bare ground, and at least some of this cover persisted through the first postfire winter rainy season. Aerial hydromulch reduced hillslope erosion from small and medium rainstorms (peak 10-minute intensities of <30 mm/hr), but not during an extreme high-intensity rain event (peak 10-minute intensity of >70 mm/hr). Hydromulch had no effect on regrowing plant cover, shrub seedling density, or species richness. Hence, in chaparral watersheds, aerial hydromulch can be an effective

postfire erosion control measure that is environmentally benign with respect to vegetation regrowth.

Keywords: wildfire, erosion control, hydromulch

Introduction

Wildfires can increase flooding and accelerate erosion in upland watersheds, adversely affecting natural resources and downstream human communities. Burned watersheds coupled with heavy winter rains can produce floods and debris flows that may affect riparian refugia of endangered species. They may also threaten life, property, and infrastructure (roads, bridges, utility lines, communication sites, pipelines) some distance from the fire perimeter. Land managers often use mitigation measures on the burned hillside slopes to reduce postfire sediment fluxes as the first step in ecosystem restoration and to protect human developments. Some of these rehabilitation treatments are costly but have not yet been proven to reduce erosion in wildland settings and may have serious consequences for postfire watershed recovery.

The physical landscape in southern California reflects the balance between active tectonic uplift and the erosional stripping of rock and soil material off the upland areas, along with the delivery of this sediment to the lowlands. Fire is a major disturbance event in southern California chaparral shrublands, and much of the erosion occurs immediately after burning. The postfire landscape, with the removal of the protective vegetation cover, is susceptible both to dry season erosion—ravel—and to wet season erosion—raindrop splash, sheetflow, and rilling (Rice 1974). Moreover, fire alters the physical and chemical properties of the soil—bulk density and water repellency—reducing infiltration and promoting surface runoff (DeBano 1981). The enhanced postfire runoff can remove additional soil material from the denuded hillsides and can mobilize sediment deposits in the stream channels

Wohlgemuth is a physical scientist and Beyers is a plant ecologist, both with the U.S. Department of Agriculture, Forest Service, Pacific Southwest Research Station, Riverside, CA 92507. Robichaud is a research engineer with the U.S. Department of Agriculture, Forest Service, Rocky Mountain Research Station, Moscow, ID 83843. Email: pwohlgemuth@fs.fed.us, jbeyers@fs.fed.us, probichaud@fs.fed.us.

to produce debris flows with tremendous erosive power (Wells 1987). Postfire erosion rates decline as the regrowing vegetation canopy and root system stabilizes the hillslopes, providing critical watershed protection (Barro and Conard 1991). In the southern California foothills, erosion is driven by winter cyclonic storms. Summer thunderstorms are rare, and snowmelt runoff is virtually nonexistent, except at the highest elevations.

Hydromulch, a slurry of paper or wood fiber that dries to a permeable crust and is used to increase groundcover, is one treatment option for reducing postfire erosion. Hydromulch has been used extensively on road cut slopes and construction sites. For burned areas with steep slopes with no road access, the hydromulch needs to be applied by fixed-wing aircraft or helicopter. The aerial hydromulch used in southern California is a wood and (or) paper mulch matrix with a non-water-soluble binder, often referred to as a bonded fiber matrix (BFM) (Hubbert 2007). The BFMs are a continuous layer of elongated fiber strands held together by a water-resistant, cross linked, hydrocolloid tackifier (bonding agent) that anchors the fiber mulch matrix to the soil surface (Hubbert 2007). BFMs provide a thicker cover than ordinary hydromulch and are recommended for steeper ground and areas frequented by high intensity storms. BFMs largely eliminate direct rain drop impact onto the soil, have high water holding capacity, are sufficiently porous not to inhibit plant growth, and will biodegrade completely. Breakdown of the product does not occur for up to 6–12 months through multiple wetting and drying cycles (Hubbert 2007).

Aerial hydromulch is a relatively new erosion control treatment that has not been extensively tested under field conditions in burned upland areas. Its ability to reduce erosion has not been quantitatively demonstrated, while its effects on regrowing vegetation are virtually unknown (Robichaud et al. 2000). The objectives of this study are to quantify the ability of aerial hydromulch to reduce postfire hillslope erosion and to document its effect on vegetation regrowth.

Study Sites

Aerial hydromulch has been used on three large wildfires located on National Forest lands in southern California in close proximity to the wildland/urban interface since 2007 (Figure 1). In each case a U.S. Department of Agriculture Forest Service Burned Area Emergency Response (BAER) team determined that

there were significant threats to life, property, and infrastructure in the downstream human communities and recommended aerial hydromulch as a postfire erosion control treatment.

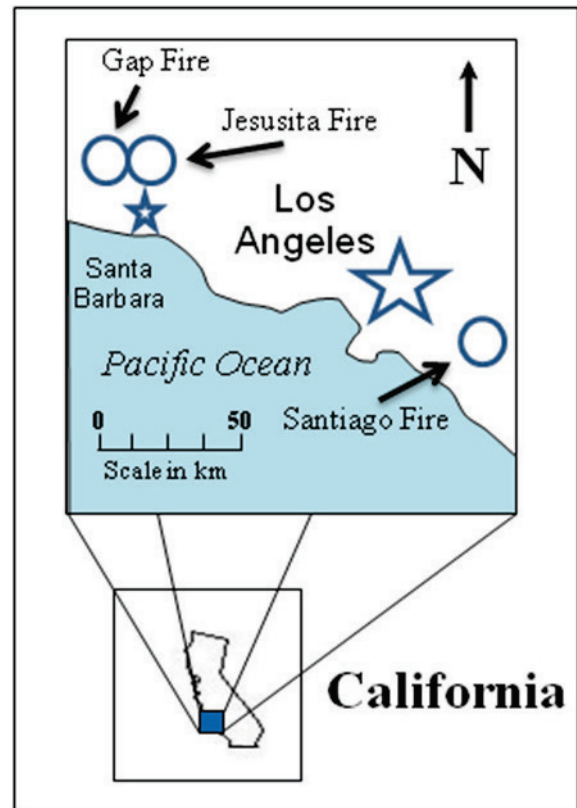


Figure 1. Location map of the study areas.

The Santiago Fire burned over 11,300 ha in Santiago Canyon, northeastern Orange County, CA (Figure 1). The burned area is a deeply dissected mountain block underlain by sedimentary and metamorphic rocks that produces a rocky, highly erosive soil (Wachtell 1975). The area was covered with thick chaparral vegetation, with some areas having no previous record of burning. Approximately 500 ha were treated with aerial hydromulch at a total cost of just under \$5 million.

The Gap Fire burned nearly 3,850 ha in the Santa Ynez Mountains in Santa Barbara County, CA, in July 2008 (Figure 1). The burned area consists of the upper half of the coastal face of a linear mountain range underlain by sedimentary rocks that produce an erosive coarse-grained soil (Shipman 1981). Prior to the fire, the area was covered with mixed chaparral. Nearly 625 ha were treated with aerial hydromulch at a total cost of just under \$5 million.

The Jesusita Fire burned roughly 3,540 ha in the Santa Ynez Mountains, Santa Barbara County, CA, in May 2009 (Figure 1). The burned area included the middle to lower slopes and canyons of the coastal face of a linear mountain range underlain by sedimentary rocks that produce an erosive coarse-grained soil (Shipman 1981). Nearly identical in site characteristics (topography, geology, soils) to the Gap Fire, the area was also covered with mixed chaparral vegetation prior to the fire. Over 80 ha were treated with aerial hydromulch at a total cost of \$640,000.

Methods

Sites were operationally treated with aerial hydromulch, and plots were established on uniform slope facets. Companion control plots were established in nearby untreated areas, ideally within a few hundred meters of the treated plots with similar site characteristics. A minimum of four raingages were deployed at each study site to measure precipitation amounts and intensities. County gages within 5 km of the sites provided long-term data to put the measured rainfall in historical context. The studies were funded to measure erosion and vegetation regrowth for 3 years after each fire.

Hillslope erosion was measured using barrier fences constructed of high tensile strength nylon landscape fabric wired to t-posts (Robichaud and Brown 2002). The sediment fences were arranged in discrete clusters on the Santiago and Gap sites and along a series of adjacent interior spur ridges at the Jesusita site. On the Gap and Jesusita sites, the sediment fence plots were bounded by an upper trench, creating an area 15–20 m in length. The plots on the Santiago site were unbounded, averaging about 55 m in length. The fences built for these studies were approximately 5 m wide and 1 m high, with the capacity of the fence determined by its height, width, and hillslope gradient. Sediment captured by the fences was cleaned out using shovels and buckets after each rainstorm or series of storms. The sediment from each fence cleanout was weighed in the field and subsampled for moisture, and the field weights were corrected to account for the weight of the water.

Cover was measured in 1 m × 1 m quadrats using a grid frame and a pointer. The pointer was lowered at 100 points in a 10 cm × 10 cm grid within each quadrat. Hits were recorded for the various classes of cover and were converted to a percentage. Groundcover categories consisted of hydromulch, organic material

(stumps, wood, live plant bases, litter), and bare soil including gravel and rocks. If the aerial hydromulch covered pieces of rock or wood, it was counted as mulch. Aerial cover from the regrowing vegetation was tallied separately from groundcover provided by plant bases. Two quadrats were initially sampled after site establishment just upslope of each sediment fence. An additional five quadrats were established for each fence in the first postfire spring season. These latter quadrats were placed from 4 to 20 m from the fence along vertical transects at the edges of each fence contributing area. Aerial plant cover was recorded by species. Surveys were conducted 2–3 times during the first postfire year, then annually in the spring. Indicators of postfire vegetation response include the amount of aerial plant cover (as opposed to groundcover), the density of shrub seedlings (the eventual climax vegetation), and a measure of species diversity or richness.

Results and Discussion

Initially, aerial hydromulch greatly reduced bare ground on the treated plots compared to the controls (Tables 1–3), presumably affording a greater level of watershed protection. Treatment cover of 17–24 percent persisted through the first postfire winter (over 65 percent on the Santiago site), but the hydromulch was less than 5 percent by the end of the second or third year after the fire. Cover of organic matter, less than 10 percent at the time of site establishment, reflected differences in rainfall as well as inherent site characteristics. Organic cover accumulated slowly on the Santiago site (which experienced a postfire drought) compared to the spectacular regrowth on the Jesusita site.

Total annual rainfall (and percent of long-term normal from nearby county gages), peak 10-minute rainfall intensity, and hillslope erosion aggregated to annual totals for treated and untreated plots are arrayed in Tables 4–6. The 64–84 percent reduction in first-year sediment yield compared to the untreated controls suggests that the aerial hydromulch was effective in controlling erosion on the Gap and Jesusita sites. At the Santiago site, initial storms of small and moderate amounts and intensities showed a reduction in hillslope erosion on the treated plots similar to the two Santa Barbara sites. However, an unusual short-duration but very high-intensity thunderstorm (>70 mm/hr) at the end of May completely overwhelmed the site, causing massive erosion to treated and untreated plots alike. Sediment fences were overtopped and the differences

in first-year erosion (Table 4) are minimum values and merely reflect the differences in fence capacity. Thus, while aerial hydromulch can reduce hillslope erosion from small and medium rainstorms, it was ineffective during an extreme high-intensity rainfall event.

The hydromulch treatment caused no substantial differences in the amount of aerial plant cover, shrub seedling density, or species richness (Tables 7–9). There was no evidence that any species were eliminated or suppressed by the presence of the hydromulch. Thus, apart from minor differences attributed to inherent site characteristics, the aerial hydromulch was environmentally benign with respect to vegetation regrowth.

Conclusions

Resources on public lands need wise management while human development requires prudent hazard protection. Both are threatened by accelerated erosion in the aftermath of wildland fire. Aerial hydromulch is a relatively new erosion control technique that was previously untested in southern California watersheds and had raised concerns about unwanted environmental side effects. A recent series of wildfires and the application of aerial hydromulch as a BAER treatment prompted this study to evaluate the effectiveness of the mulch in reducing erosion and its affect on regrowing chaparral vegetation.

The aerial hydromulch does increase groundcover, some of which persists through the first postfire rainy season. The aerial hydromulch reduced hillslope erosion by 64–84 percent compared to untreated controls for small and moderate rainstorms, but not for an extreme rainfall event (>70 mm/hr). Moreover, the aerial hydromulch appeared to have no affect on postfire vegetation cover or species richness. Thus, in southern California chaparral watersheds, aerial hydromulch appears to be an effective postfire erosion control treatment from all but the largest storms and is environmentally benign with respect to vegetation regrowth.

Table 1. Average groundcover—Santiago Fire.

Survey	Hydromulch (n=10) (%)	Control (n=10) (%)
Site establishment		
Treatment	66.0	0
Organics	0.8	2.1
Bare soil	33.2	97.9
Year 1		
Treatment	65.7	0
Organics	3.1	2.8
Bare soil	31.2	97.2
Year 2		
Treatment	18.4	0
Organics	27.8	20.5
Bare soil	53.8	79.5
Year 3		
Treatment	3.6	0
Organics	64.0	41.7
Bare soil	32.4	58.3

Table 2. Average groundcover—Gap Fire.

Survey	Hydromulch (n=10) (%)	Control (n=6) (%)
Site establishment		
Treatment	87.8	1.7
Organics	1.2	2.4
Bare soil	11.0	95.9
Year 1		
Treatment	24.9	0
Organics	21.0	17.0
Bare soil	54.1	83.0
Year 2		
Treatment	0.6	0
Organics	72.6	83.7
Bare soil	26.8	16.3

Table 3. Average groundcover—Jesusita Fire.

Survey	Hydromulch (n=10) (%)	Control (n=9) (%)
Site establishment		
Treatment	80.6	0
Organics	10.2	11.0
Bare soil	9.2	89.0
Year 1		
Treatment	17.7	0
Organics	66.7	62.6
Bare soil	15.6	37.4

Table 4. Average hillslope erosion—Santiago Fire.

Collection period	Hydromulch (n=10)	Control (n=10)
Year 1		
TAR	275 (59%)	
I ₁₀	70.1	
HE	20.67*	26.1*
Year 2		
TAR	336 (64%)	
I ₁₀	38.6	
HE	6.4	8.6
Year 3		
TAR	547 (93%)	
I ₁₀	58.8	
HE	10.3	10.8

TAR, total annual rainfall (mm) (percent of normal)

I₁₀, peak 10-minute intensity (mm/hr)

HE, hillslope erosion (Mg/ha)

*Minimum value (fences overtopped)

Table 5. Average hillslope erosion—Gap Fire.

Collection period	Hydromulch (n=10)	Control (n=6)
Year 1		
TAR	469 (54%)	
I ₁₀	59.4	
HE	7.8	21.5
Year 2		
TAR	1,055 (113%)	
I ₁₀	27.4	
HE	2.8	5.1

TAR, total annual rainfall (mm) (percent of normal)

I₁₀, peak 10-minute intensity (mm/hr)

HE, hillslope erosion (Mg/ha)

Table 6. Average hillslope erosion—Jesusita Fire.

Collection period	Hydromulch (n=10)	Control (n=9)
Year 1		
TAR	554 (87%)	
I ₁₀	41.1	
HE	5.3	33.7

TAR, total annual rainfall (mm) (percent of normal)

I₁₀, peak 10-minute intensity (mm/hr)

HE, hillslope erosion (Mg/ha)

Table 7. Average vegetation response—Santiago Fire.

Survey	Hydromulch (n=10)	Control (n=10)
Year 1		
APC	13.1	20.9
SSD	NA	NA
SR	1.7	3.2
Year 2		
APC	95.0	99.5
SSD	2.6	2.7
SR	4.1	5.5
Year 3		
APC	141.5*	115.4*
SSD	NA	NA
SR	8.4	10.5

APC, aerial plant cover (percent)

SSD, shrub seedling density (seedlings per quadrat)

SR, species richness (species per quadrat)

*overlapping plant cover can exceed 100 percent

Table 8. Average vegetation response—Gap Fire.

Survey	Hydromulch (n=10)	Control (n=6)
Year 1		
APC	75.3	47.0
SSD	6.9	6.4
SR	6.2	3.2
Year 2		
APC	160.4*	143.9
SSD	4.8	5.3
SR	9.8	6.8

APC, aerial plant cover (percent)

SSD, shrub seedling density (seedlings per quadrat)

SR, species richness (species per quadrat)

* overlapping plant cover can exceed 100 percent

Table 9. Average vegetation response—Jesusita Fire.

Survey	Hydromulch (n=10)	Control (n=9)
Year 1		
APC	155.3	158.7*
SSD	7.5	3.2
SR	7.4	8.4

APC, aerial plant cover (percent)

SSD, shrub seedling density (seedlings per quadrat)

SR, species richness (species per quadrat)

* overlapping plant cover can exceed 100 percent

Acknowledgments

The authors appreciate the reviews of Lee MacDonald and Dan Neary. These studies were funded by the U.S. Department of Agriculture Forest Service, National Burned Area Emergency Response Program.

References

- Barro, S.C., and S.G. Conard. 1991. Fire effects on California chaparral systems: An overview. *Environment International* 23:135–149.
- DeBano, L.F. 1981. Water repellent soils: A state-of-the-art. U.S. Department of Agriculture, Forest Service, General Technical Report PSW-46.
- Hubbert, K.R. 2007. Treatment effectiveness monitoring for southern California wildfires. Report to the U.S. Department of Agriculture, Forest Service, Region 5, Vallejo, CA, 126 pp.
- Rice, R.M. 1974. The hydrology of chaparral watersheds. In M. Rosenthal, ed. *Proceedings of the Symposium on Living with the Chaparral*, Riverside, CA, 30–31 March 1973, pp. 27–34. Sierra Club, San Francisco, CA.
- Robichaud, P.R., J.L. Beyers, and D.G. Neary. 2000. Evaluating the effectiveness of postfire rehabilitation treatments. U.S. Department of Agriculture, Forest Service, General Technical Report RMRS-63.
- Robichaud, P.R., and R.E. Brown. 2002. Silt fences: An economical technique for measuring hillslope erosion. U.S. Department of Agriculture, Forest Service, General Technical Report RMRS-GTR-94.
- Shipman, G.E. 1981. Soil survey of Santa Barbara County, California, south coastal part. U.S. Department of Agriculture, Soil Conservation Service and Forest Service, 156 pp.
- Wachtell, J.K. 1975. Soil survey of Orange County and western part of Riverside County, California. U.S. Department of Agriculture, Soil Conservation Service and Forest Service, 149 pp.
- Wells, W.G., II. 1987. The effects of fire on the generation of debris flows in southern California. *Geological Society of America, Reviews in Engineering Geology* 7:105–114.

Remote Sensing of Soil Tillage Intensity in a CEAP Watershed in Central Iowa

C.S.T. Daughtry, P.C. Beeson, S. Milak, B. Akhmedov, E.R. Hunt Jr., A.M. Sadeghi, M.D. Tomer

Abstract

Crop residues on the soil surface decrease soil erosion, increase water infiltration, increase soil organic matter, and improve soil quality. Thus, management of crop residues is considered an integral part of most conservation tillage systems. Crop residue cover is used to classify soil tillage intensity and assess the extent of conservation tillage practices. Our objectives were (1) to review remote sensing methods for assessing crop residue cover and soil tillage intensity, and (2) to examine process models for assessing the effects of crop management decisions on soil and water quality.

The spectral properties of crop residues and soils in crop production fields in Maryland, Indiana, and Iowa were measured with ground-based spectroradiometers and airborne and satellite imaging spectrometers. Physically-based spectral indices that detect absorption features associated with cellulose and lignin were robust and required minimal surface reference data for mapping soil tillage intensity across agricultural landscapes. Stratified sampling protocols are needed that use a limited number of hyperspectral images to provide reliable data for training classifiers of widely available multispectral images.

The South Fork watershed is a Conservation Effects Assessment Project (CEAP) watershed in central Iowa. Farmer surveys, surface reference data, and remotely sensed data provided spatially-explicit input data for

Daughtry is a research agronomist, Beeson is a hydrologist, Hunt is a physical scientist, and Sadeghi is a soil physicist, all with the U.S. Department of Agriculture–Agricultural Research Service, Hydrology and Remote Sensing Laboratory, Beltsville, MD 20705. Milak is a senior engineer and Akhmedov is a lead engineer, both with Science Systems and Applications, Inc., Lanham, MD 20706. Tomer is a soil scientist with the U.S. Department of Agriculture–Agricultural Research Service, Laboratory for Agriculture and the Environment, Ames, IA 50011. Email: craig.daughtry@ars.usda.gov.

hydrologic and soil carbon models. Crop and soil management scenarios were evaluated using watershed- and field-scale models. An interconnected suite of models is required to address the wide range of agronomic, environmental, and economic questions likely to be posed by farmers, stakeholders, and policymakers related to harvesting crop residues for biofuels.

Keywords: crop residue cover, remote sensing, SWAT, EPIC, water quality, soil erosion, CEAP

Introduction

Crop residues on the soil surface can decrease soil erosion and runoff, increase soil organic matter, improve soil quality, increase water infiltration, and reduce the amounts of nutrients and pesticides that reach streams and rivers (Lal et al. 1999). Three useful categories of tillage based on crop residue cover after planting have been defined: intensive tillage has <15 percent residue cover; reduced tillage has 15–30 percent residue cover; and conservation tillage has >30 percent residue cover (Daughtry et al. 2006). Thus, quantification of crop residue cover is required to evaluate the effectiveness and extent of conservation tillage practices as well as the extent of biofuel harvesting. For agricultural fields, the standard technique for measuring crop residue cover is the line-point transect method, which is time consuming and prone to errors (Morrison et al. 1993).

Remote sensing approaches for assessing soil tillage intensity and crop residue cover have frequently used broadband multispectral sensors, such as Landsat Thematic Mapper (TM). Within these broad bands, crop residues and soils are spectrally similar and often differ only in amplitude. Crop residue can be brighter or darker than soils depending on soil type, crop type, moisture content, and residue age (Daughtry and Hunt 2008), making it difficult to distinguish residues from soils.

With hyperspectral reflectance data, three relatively narrow absorption features—centered near 1,730, 2,100, and 2,300 nm—can be detected that are primarily associated with nitrogen, cellulose, and lignin concentrations. These features are not readily discernible in the spectra of fresh vegetation, but they are evident in reflectance spectra of dry non-photosynthetic vegetation, including crop residues. Reflectance spectra of dry soils also lack these absorption features but may have additional absorption features associated with minerals (Serbin et al. 2009 a).

Our objectives were (1) to review remote sensing methods for assessing crop residue cover and soil tillage intensity, and (2) to examine process models for assessing the effects of crop management decisions on soil and water quality. We started with the fundamental spectral properties of crop residues and soils, extended the results to fields and watersheds, and finally simulated the effects of biofuel harvesting on soil erosion and soil C.

Materials and Methods

Laboratory to Small Plot Scales

Reflectance spectra were acquired with a FieldSpec Pro spectroradiometer (Analytical Spectral Devices, Boulder, CO), equipped with an 8°-fore optic, over the 350–2,500-nm wavelength region. The samples were illuminated by six 100-W quartz-halogen lamps mounted on the arms of a camera copy stand and stabilized by a current-regulated power supply. A Spectralon reference panel (Labsphere, Inc, North Sutton, NH,) was also measured and reflectance factors were calculated (Walter-Shea and Biehl 1990).

Crop residues of corn (*Zea mays* L.), soybean (*Glycine max* Merr.), and wheat (*Triticum aestivum* L.) were collected from fields near Beltsville, MD, at 1 week and 7 months after harvest. Spectral reflectance of the intact dry crop residues were measured in 45 × 45 cm sample trays filled to a depth of 2 cm.

To provide a wide range of soil colors, the topsoils for this study included Loring (fine-silty, mixed, active, thermic Oxyaquic Fragiudalfs) from Como, MS; Sverdrup (sandy mixed, frigid, Typic Hapludolls) from Morris, MN; and Gaston (fine, mixed, active, thermic Humic Hapludults) from Salisbury, NC. Each soil was dried, crushed to pass a 2-mm screen, and placed in 45-cm sample trays to a depth of 2 cm.

Reflectance spectra of crop residues and soils were acquired in situ from production fields in Maryland, Indiana, and Iowa. The 18°-fore optic of the spectroradiometer and a digital camera were mounted on a pole and positioned at 2.3 m above the soil at a 0° view zenith angle. A Spectralon reference panel was also measured and reflectance factors were calculated. Crop residue cover within the field of view of the spectroradiometer was assessed visually with a dot-grid overlay (Daughtry and Hunt 2008).

The cellulose absorption index (CAI) approximated the depth of the 2,100-nm feature using three narrow spectral bands (Daughtry and Hunt 2008). The CAI = $100(0.5(R_{2,0} + R_{2,2}) - R_{2,1})$, where $R_{2,0}$, $R_{2,1}$, and $R_{2,2}$ refer to reflectance values in 10-nm bands centered at 2,030 nm, 2,100 nm, and 2,210 nm, respectively.

Field to Watershed Scales

Airborne hyperspectral images were acquired using a ProspecTIR VS System (SpecTIR LLC, Sparks, NV) over 5 test sites in Maryland, Indiana, and Iowa (Serbin et al. 2009 b). The images covered the 450–2,500-nm wavelength region at approx. 5-nm intervals with a 4-m spatial resolution. The Hyperion imaging spectrometer on the NASA Earth Observing-1 spacecraft acquired images over test sites in Iowa that included the Walnut Creek watershed (Daughtry et al. 2006) in 2004 and 2005 and the South Fork watershed (Tomer et al. 2008) in 2009 and 2011. The images covered the 400–2,500-nm wavelength region at approx. 10-nm intervals with a 30-m spatial resolution. Landsat TM multispectral images were also acquired.

For each test site and year, crop residue cover was determined in over 50 corn and soybean fields using the line-point transect method (Daughtry et al. 2006). The distributions of crops for each test site and year were extracted from the Cropland Data Layer product (Johnson and Mueller 2010). Corn and soybeans accounted for >90 percent of the cropland in each test site.

South Fork Watershed

The South Fork watershed of the Iowa River covers about 788 km² and is part of the U.S. Department of Agriculture Conservation Effects Assessment Project (CEAP) (Duriancik et al. 2008). The watershed is dominated by pothole depressions and subsurface tile drainage is needed to drain the hydric soils that cover 54 percent of the watershed (Tomer et al. 2008). The watershed is 84 percent cropland, and the rest is mostly

pasture or forest with very limited urban areas. Corn and soybeans are grown on more than 99 percent of the cropland area. Temporal and geospatial data for the watershed include soil properties, climate, crop classification, and management practices.

Results and Discussion

Laboratory to Plot-Scales

The mean reflectance spectra of crop residues and soils have similar shapes (Figures 1, 2). Closer examination of the 2,000–2,400-nm regions reveals two broad absorption features that are primarily associated with cellulose and lignin. As the crop residues decomposed and the relative proportions of lignin, cellulose, and other structural polysaccharides changed, the intensities of these absorption features diminished (Daughtry et al. 2010).

The spectra of three diverse agricultural soils lack the absorption features associated with cellulose and lignin but have absorption features near 2,200 nm that are associated with clay minerals (Figure 2). Kaolinite (clay), with its characteristic doublet absorption feature at 2,150 nm and 2,200 nm, is the dominant mineral in the Gaston (Ultisol) soil spectrum (Serbin et al. 2009 a). The single absorption feature at 2,200 nm is associated with illite and montmorillonite clays.

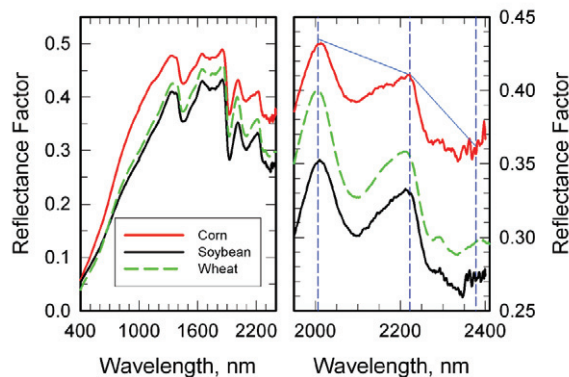


Figure 1. Reflectance spectra of corn, soybean, and wheat residues collected from fields 7 months after harvest. Absorption features near 2,100 nm and 2,300 nm are associated with cellulose and lignin. Reflectance is less than the continuum line (blue) for each feature.

Crop residue cover was linearly related to CAI from ground-based reflectance data (Figure 3A) and provided more robust assessments of crop residue cover for the diverse soils than the Landsat TM band

residue/tillage indices (Serbin et al. 2009 b). Similar results have been reported for other crop residue and soil combinations.

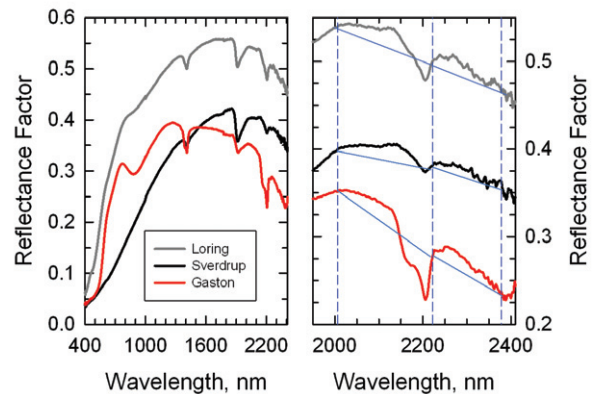


Figure 2. Reflectance spectra of three diverse agricultural soils. Absorption features near 2,200 nm are associated with clay mineralogy. Reflectance is greater than the continuum line (blue) except near 2,200 nm.

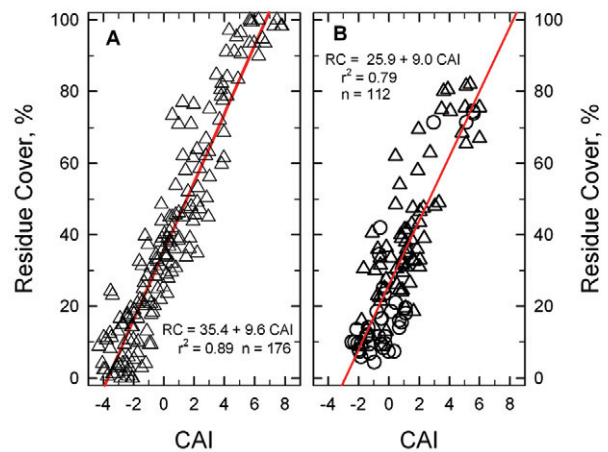


Figure 3. Crop residue cover as a linear function of CAI for (A) ground-based ASD spectroradiometer and (B) satellite-based Hyperion imaging spectrometer data.

Field to Watershed Scales

Crop residue cover was also linearly related to CAI from satellite reflectance data (Figure 3B). Corn fields typically had more residue cover than soybean fields; however, crop type did not significantly affect the slope of the regression lines. Other years and test sites had similar relationships (Table 1), which indicates that the crop residue cover versus CAI relationship is stable and robust (Daughtry et al. 2006, Serbin et al. 2009 b).

Shifts in soil tillage intensity over time and space can be tracked by combining georeferenced information on previous crops from the Cropland Data Layer with georeferenced information on crop residue cover. For example, 37 percent of the cropland in the Walnut Creek test site was classified as conservation tillage (>30 percent cover) in 2004 compared with 65 percent conservation tillage in 2005 (Table 2). This large shift in the proportion of conservation tillage may be related to spring weather conditions. Spring 2004 weather was warm and dry, which allowed ample time for additional tillage, but spring 2005 weather was cool and wet, which reduced opportunities for tillage and encouraged farmers to plant as quickly as possible.

Table 1. Sensors, locations, and statistics for crop residue cover as a linear function of CAI. Within a sensor, changes in slope are related to scene moisture.

Sensor	Loc	Date	Slope	RMSE	R ²
ProspecTIR	IN	2006	23.1	0.12	0.80
	IN	2007	27.6	0.11	0.83
	IA	2007	23.8	0.08	0.83
Hyperion	IA	2004	9.0	0.10	0.79
	IA	2005	12.3	0.15	0.65

Table 2. Percent of crop acreage in three soil tillage intensity classes. Tillage intensity is based on crop residue cover estimated using Hyperion imagery acquired shortly after planting for test sites in Iowa. Tillage classes are intensive tillage (IT) with <15 percent residue cover; reduced tillage (RT) with 15–30 percent residue cover; and conservation tillage (CT) with >30 percent residue cover.

Previous crop	3 May 2004			22 May 2005		
	IT	RT	CT	IT	RT	CT
Corn	18	36	46	7	38	55
Soybean	35	40	25	3	21	76
Total	25	38	37	5	30	65

Watershed-Scale Simulations

Currently, remote sensing cannot directly assess soil carbon (except at the soil surface), or water quality (except as turbidity and color); however, remote sensing can provide some of the biophysical variables, including soil and crop management practices and local topography, needed by physically-based process models to predict carbon dynamics and water quality across agricultural landscapes. These process-based models can provide accurate estimates of soil erosion

and nutrient loading, which are both major components of carbon dynamics and water quality.

Remote sensing offers a practical method to account for the spatial and temporal variability inherent across agricultural landscapes. However, current hyperspectral sensors have a very narrow swath and do not have the capacity to map watersheds in a timely manner. Therefore, the challenge is how to best use a few hyperspectral images and many multispectral images to produce regional surveys and maps of crop residue cover and tillage intensity.

The Soil and Water Assessment Tool (SWAT) is a quasi-physically-based water quality simulation model that predicts the effect of management on water, sediment, and agricultural chemical yields in watersheds (Arnold et al. 1998). After successful model calibration, sediment discharges predicted by SWAT were well correlated with sediment discharges measured near the outlet of the South Fork watershed (Beeson et al., in press).

SWAT estimated annual sediment discharge for the South Fork watershed using three different scenarios of soil tillage intensity— (1) all fields with conventional tillage (<30 percent residue cover); (2) all fields with conservation tillage (≥30 percent cover); and (3) all fields with no tillage (except for planting and fertilizer applications; >60 percent cover). In addition, two different above ground residue removal rates (0 and 80 percent) were simulated for each tillage scenario.

Water quality as measured by sediment discharge in the South Fork river is strongly affected by the amount of precipitation received. Our simulation results revealed that sediment discharge in a wet year, such as 2008, was an order of magnitude greater than the sediment load in a normal year (Figure 4). Because of the environmental risks associated with above normal precipitation, proactive management strategies for the South Fork watershed should encourage reducing soil tillage intensity to maintain crop residue cover on the soil and establishing filter strips to retain sediment. Residue removal increased the amount of sediment discharge from the watershed because of the decreased infiltration and reduced cover on the soil surface.

Field-Scale Simulations

The Erosion Productivity Impact Calculator (EPIC) is an ecosystem model capable of simulating many processes in agricultural land such as crop growth and

yield, water balance, and nutrient cycling as affected by weather, soil, and management practices (Williams et al. 1984). EPIC is well suited for addressing the effects of crop and soil management practices at the individual field unit. A series of EPIC simulations evaluated the effects of management practices on soil sustainability over time.

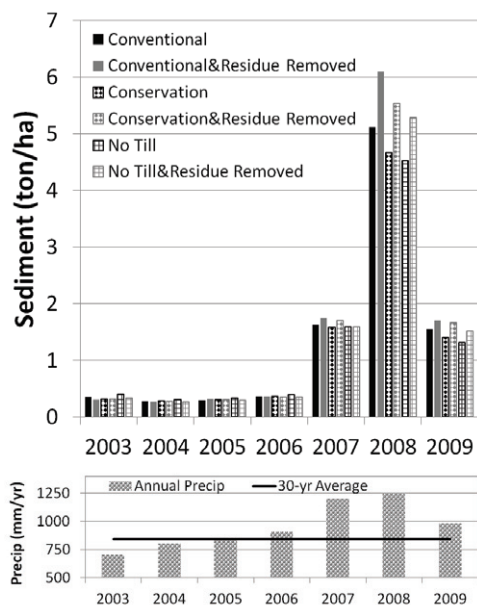


Figure 4. SWAT simulations of annual sediment discharge at the outlet of the South Fork watershed for 6 management scenarios (2003–2009). Each scenario included continuous corn with different tillage intensities and residue removal rates.

As a case study, we considered the following scenario: a farmer in the South Fork watershed has two fields with different dominant soil types. Both fields have similar topographic relief (about 2 percent slope) and have grown corn continuously with conventional tillage for several years. The dominant soil in one field is a loam and the other field is a silty clay loam (Table 3). The farmer would like to evaluate the effects of harvesting corn residues for biofuel and changing tillage practices on the stable soil carbon in the top 20 cm of each soil and the sediment loss in each field over the next 10 years. His tillage options are to continue with the conventional tillage program (<30 percent crop residue cover) or switch to a no-till program. Biofuel harvesting would remove 80 percent of the corn residue remaining on the soil surface after corn grain harvest.

After 10 years of simulations, the stable organic carbon in the top 20 cm of these soils increased and the soil loss decreased as soil tillage intensity changed from conventional tillage to no-till (Table 3). Conventional

tillage with crop residue removal reduced soil organic carbon and increased soil loss from both soils, particularly for the field with silty clay loam soil. The positive effects of switching from conventional tillage to no-till more than offset any losses due to crop residue removal for both soils. These simulations indicate that removal of up to 80 percent of the corn residue from these two nearly flat soils is sustainable if tillage intensity is reduced by switching from conventional tillage to no-till management.

Table 3. EPIC simulated changes in stable carbon pools and annual sediment loss from a silty clay loam (SCL) and a loam soil in the South Fork watershed after 10 years with different management scenarios.

Soil texture	Tillage intensity	Initial conditions	Residue removal	
			0%	80%
Stable soil carbon, t/ha				
SCL	Conventional	92.5	93.5	88.5
	No-till	92.5	96.1	93.3
Loam	Conventional	66.1	67.8	63.8
	No-till	66.1	70.4	67.3
Annual sediment loss, t/ha				
SCL	Conventional	2.3	2.8	6.1
	No-till	2.3	0.5	1.1
Loam	Conventional	2.6	3.0	6.1
	No-till	2.6	0.6	1.1

These EPIC model simulations demonstrated that the environmental effects of crop residue removal can be minimal in some geographic areas. However, as slope increased, the amount of crop residue that can be harvested in a sustainable manner is much lower. For other geographic regions, the effects of residue removal can be different. For example, corn residue harvest adversely affected soil organic carbon of the loamy sand soils of the Coastal Plain region of the southeastern United States (Gollany et al. 2010).

Well validated models can be valuable tools for evaluating management practices for a given soil-climate-crop combination that maximize biomass production and minimize environmental effects. Spatial and temporal variability at field and landscape scales is great and a robust decision support system must include a suite of models to address the wide range of agronomic, environmental, and economic questions likely to be posed by farmers, stakeholders, and policy makers. The issues to be addressed and the level of detail (spatial and temporal resolution) required would determine which model of the suite should be used.

Conclusions

While in situ measurements can accurately describe conditions in plots and small fields, remote sensing offers a practical method to account for the spatial variability inherent across agricultural landscapes. Many of the biophysical characteristics of vegetation and soils that are needed by field-and watershed-scale process models can be derived directly or indirectly from remotely sensed data.

Currently, remote sensing systems are constrained by compromises in spatial and temporal resolution. However, data fusion and data assimilation techniques have shown considerable promise for merging data from multiple sources and creating synthetic datasets with enhanced spatial and temporal resolutions. Based on the field and watershed scenarios evaluated, process models of varying scales together with these enhanced datasets appear to provide much better descriptions of ecosystem functions at field to national scales.

References

- Arnold, J.G., R. Srinivasan, R.S. Muttiah, and J.R. Williams. 1998. Large-area hydrologic modeling and assessment: Part I. Model development. *Journal of the American Water Resources Association* 34:73–89.
- Beeson, P.C., P.C. Doraiswamy, A.M. Sadeghi, M. DiLuzio, M.D. Tomer, J.G. Arnold, and C.S.T. Daughtry. In press. Treatments of precipitation inputs to SWAT models. *Transactions of the American Society of Agricultural and Biological Engineers*.
- Daughtry, C.S.T., P.C. Doraiswamy, E.R. Hunt, Jr., A.J. Stern, J.E. McMurtrey, III, and J.H. Prueger. 2006. Remote sensing of crop residue cover and soil tillage intensity. *Soil Tillage Research* 91:101–108.
- Daughtry, C.S.T., and E.R. Hunt, Jr. 2008. Mitigating the effects of soil and residue water contents on remotely sensed estimates of crop residue cover. *Remote Sensing of Environment*, 112:1647–1657.
- Daughtry, C.S.T., G. Serbin, J.B. Reeves, III, P.C. Doraiswamy, and E.R. Hunt, Jr. 2010. Effects of decomposition of remotely sensed estimates of wheat residue cover. *Remote Sensing* 2:416–431.
- Duriancik, L.F., D. Bucks, J.P. Dobrowolski, T. Drewes, S.D. Eckles, L. Jolley, R.F. Kellogg, D. Lund, J.R. Makuch, M.P. O'Neill, C.A. Rewa, M.R. Walbridge, R. Parry, and M.A. Weltz. 2008. The first five years of the Conservation Effects Assessment Project. *Journal of Soil and Water Conservation* 63:185A–197A.
- Gollany, H.T., J.M. Novak, Y. Liang, S.L. Albrecht, R.W. Rickman, R.F. Follet, W.W. Wilhelm, and P.G. Hunt. 2010. Simulating soil organic carbon dynamics with residue removal using the CQESTR model. *Soil Science Society of America Journal* 74:372–383.
- Johnson, D.M., and R. Mueller. 2010. The 2009 Cropland Data Layer. *Photogrammetric Engineering and Remote Sensing* 76:1201–1205.
- Lal, R., J.M. Kimble, R.F. Follett, and C.V. Cole. 1999. *The Potential of U.S. Cropland to Sequester Carbon and Mitigate the Greenhouse Effect*. Lewis Publishers, Boca Raton, FL.
- Morrison, J.E., C. Huang, D.T. Lightle, and C.S.T. Daughtry. 1993. Residue cover measurement techniques. *Journal of Soil and Water Conservation* 48:479–483.
- Serbin, G., C.S.T. Daughtry, E.R. Hunt, Jr., D.J. Brown, and G.W. McCarty. 2009a. Effect of soil spectral properties on remote sensing of crop residue cover. *Soil Science Society of America Journal* 73:1545–1558.
- Serbin, G., E.R. Hunt, Jr., C.S.T. Daughtry, G.W. McCarty, and P.C. Doraiswamy. 2009b. An improved ASTER index for remote sensing of crop residue. *Remote Sensing* 1:971–991.
- Tomer, M.D., T.B. Moorman, and C.G. Rossi. 2008. Assessment of the Iowa River's South fork watershed: 1. Water quality. *Journal of Soil and Water Conservation* 63:360–370.
- Walter-Shea, E.A., and L.L. Biehl. 1990. Measuring vegetation spectral properties. *Remote Sensing Reviews* 1:179–206.
- Williams, J.R., C.A. Jones, and P.T. Dyke. 1984. A modeling approach to determining the relationship between erosion and soil productivity. *Transactions of the American Society of Agricultural Engineers* 27:129–144.

Spatiotemporal Analysis of Surface and Subsurface Soil Moisture for Remote Sensing Applications within the Upper Cedar Creek Watershed

Gary C. Heathman, Michael H. Cosh, Eunjin Han, Venkatesh Merwade, Thomas J. Jackson

Abstract

Soil moisture is a key state variable that varies considerably in space and time. From a hydrologic viewpoint, soil moisture controls runoff, infiltration, storage, and drainage. Soil moisture determines the partitioning of the incoming radiation between latent and sensible heat fluxes. Although soil moisture is highly variable, if measurements of soil moisture at the field or small watershed scale are repeatedly observed, certain locations often can be identified as being temporally stable and representative of an area average. Temporal stability analysis (TSA) is a statistical approach for describing the persistence of spatial patterns and characteristic behavior of soil moisture. Using TSA, this study was aimed at determining the adequacy of long-term point-scale surface and subsurface soil moisture (θ_v) measurements in representing field- and watershed-scale averages that will serve as in situ ground truth locations for remotely sensed soil moisture calibration and validation programs, as well as applications for hydrologic modeling. Spatiotemporal analysis revealed persistent patterns in surface soil moisture and identified sites that were temporally stable at both study scales. However, soil water patterns differed between preferred states (wet/dry) and were primarily controlled by lateral and vertical fluxes, respectively. At the field scale,

locations that were optimal for estimating the area average water contents were different from permanent sensor locations. However, minimum offset values could be applied to the permanent sensor data to obtain representative field average values of surface θ_v . A TSA of 20-cm θ_v showed little correlation with surface θ_v . TSA results in terms of comparable stable sites at either scale. The results are of relevance for interpreting and downscaling coarser resolution soil moisture data such as that retrieved from remotely sensed active and passive microwave platforms and in terms of modeling soil moisture at multiple scales.

Keywords: soil moisture, temporal stability, remote sensing, NASA, SMAP

Introduction

From a hydrologic viewpoint, soil moisture is the main source of memory that controls runoff, infiltration, storage, and drainage. It is a key state variable of the hydrologic cycle that varies in space and time. In meteorology, soil moisture determines the partitioning of the incoming radiation between latent and sensible heat flux and plays a crucial role in the land surface and atmospheric feedback system. From an agricultural aspect, soil moisture controls irrigation scheduling and yield forecasting. Implicit in the above mentioned is recognition that the land surface and atmosphere, as well as groundwater storage, are inextricably linked to the soil water content; therefore, detailed information of the soil water content and its spatiotemporal dynamics are necessary for sustained agricultural production, soil resource conservation, and efficient management of water resources in streams and reservoirs (Starks et al. 2003).

Heathman is a soil scientist with the U.S. Department of Agriculture–Agricultural Research Service, National Soil Erosion Research Laboratory, West Lafayette, IN 47907. Email: gary.heathman@ars.usda.gov. Cosh and Jackson are hydrologists with the U.S. Department of Agriculture–Agricultural Research Service, Hydrology and Remote Sensing Laboratory, Beltsville, MD 20705. Han is a graduate student and Merwade is a professor, both with Purdue University, Civil Engineering Department, West Lafayette, IN 47907.

At present, point-scale ground-based measurements of soil moisture are typically obtained using periodic gravimetric sampling, neutron attenuation, time-domain reflectometry (TDR), or frequency-domain reflectometry (FDR). Typically, the large spatial and temporal variability of soil moisture is not well represented with these methods. At larger scales, however, remote sensing (RS) techniques have demonstrated that spatial and temporal characterizations of surface soil moisture fields can be estimated to augment sparsely distributed point measurements from in situ networks (Njoku et al. 2002).

Several in situ studies have been designed to determine the footprint scale mean values to validate remotely sensed soil moisture products (Njoku et al. 2002, Cosh et al. 2004, Cosh et al. 2006). In situ observations are usually made point-wise, but the problem in using point measurements for validation of a measurement over a sizeable footprint is the representativeness of those point measurements with respect to the footprint measurement. In order to use the point measurements for the validation of the footprint measurement, a scaling methodology must be used. Thus, the need for better estimates of surface, as well as profile soil moisture, has heightened interest in a combination of techniques that evaluate the spatial and temporal characteristics of surface soil moisture. One approach that has been successfully used is temporal stability analysis (Vachaud et al. 1985, Cosh et al. 2004). Although surface soil moisture is highly variable, if measurements of soil moisture at the field or small watershed scale are repeatedly observed, certain locations often can be identified as being temporally stable and representative of the an area average (Vachaud et al. 1985). However, using this approach for validation has not been without errors due to limited sample size and the mismatch between point-scale field studies and the sensor footprint which may limit practical application of remotely sensed soil moisture products. Additional statistical tools may be used to characterize the sampling points to establish reliable scaling methodology. For example, a geophysical model can be used to characterize the area and to relate the point measurements to the regions whose relevance and representativeness can be evaluated through the model (Crow et al. 2005).

Our current study is, in part, one of a series of spatiotemporal studies to more effectively characterize an in situ soil moisture network in preparation for prelaunch and postlaunch National Aeronautics and Space Administration (NASA) Soil Moisture

Active/Passive (SMAP) Cal/Val field activities. The objective of this study was to determine the adequacy of long-term point-scale soil moisture measurements at depths of 5 and 20 cm to represent field- and watershed-scale averages within an agricultural watershed and thus to better characterize and quantify interactions between surface and subsurface soil moisture spatiotemporal dynamics at multiple scales. This, in turn, should improve our efforts to link point-scale measurements of soil moisture to field- and watershed-scale soil moisture dynamics, on the order of 1 to 7,000 ha in size, and should provide greater confidence in calibrating and validating remotely sensed observations because of the enhanced area of representative measurement.

Methods

Study Area and in situ Soil Monitoring Network

The experimental monitoring network shown in Figure 1 is maintained by the U.S. Department of Agriculture–Agricultural Research Service (USDA–ARS) and is located within the 19,200-ha Upper Cedar Creek watershed (UCCW) of northeastern Indiana (41°27'38.11777" N. by 84°58'30.09636" W.).

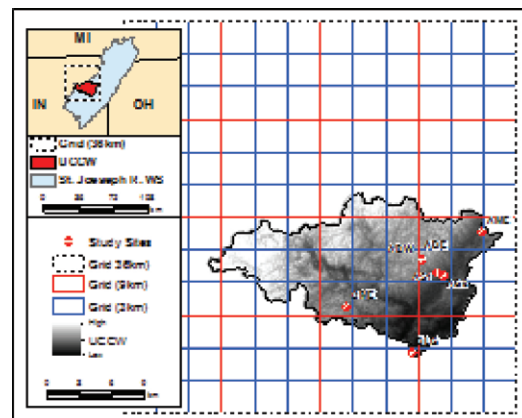


Figure 1. Upper Cedar Creek watershed study area within the St. Joseph River watershed.

The watershed monitoring network is part of the USDA's nationwide Conservation Effects Assessment Project (CEAP). The predominant land use in the UCCW is agricultural (79 percent), with major crops of corn and soybeans and minor crops of winter wheat, oats, alfalfa, and pasture. In situ soil moisture measurements were obtained from permanently installed sensors at depths of 5, 20, 45, and 60 cm at seven sites located within the UCCW monitoring network in northeastern Indiana (Figure 1). In two

agricultural fields (AS1, AS2), twenty additional soil moisture sensors spaced 70 m apart were installed at depths of 5 and 20 cm in each field with automated data collection being transmitted every 30 min from June 29 through September 21, 2010. Both fields are in a corn/soybean rotation with the AS1 field being no-till (NT) and the AS2 having rotational tillage (RT) each spring in years when corn is planted. In 2010 both fields were planted to corn in April. The predominant soils at the field sites have been classified as a Glynwood silt loam (Fine, illitic, mesic Aquic Hapludalfs) in the 2.23-ha AS1 field and as a Blount silt loam (Fine, illitic, mesic, Aeric Epiaqualfs) in the 2.71-ha AS2 field. A list of soil properties with depth for each field is given in Table 1.

Table 1. Field site soil properties.

Soil properties						
Field site	Depth (cm)	%Sand	%Clay	%Silt	Texture name	Bulk density (g/cm ³)
AS1	0–5	51.25	17.13	31.63	loam	1.42
	5–15	42.33	20.66	37.02	loam	1.42
	15–30	37.64	26.03	36.33	loam	1.49
	30–45	45.71	30.93	23.36	sandy clay loam	1.44
	45–60	36.38	36.50	27.13	clay loam	1.48
AS2	0–5	34.23	21.69	44.08	loam	1.39
	5–15	27.69	26.35	45.96	loam	1.39
	15–30	25.37	33.35	41.29	clay loam	1.53
	30–45	26.29	38.04	35.68	clay loam	1.40
	45–60	25.05	39.43	35.52	clay loam	1.38

For this study, all measurements of soil moisture are based on the frequency-domain reflectometry method of measuring the dielectric permittivity of soil to determine volumetric soil water content. As described in the manufacturer's soil sensor manual (Stevens Water Monitoring Systems, Inc., Portland, OR), the Steven's Hydra Probe II (HP-II) sensor consists of a 4-cm-diameter cylindrical head that has four 0.3-cm-diameter tines that protrude 5.8 cm. A 50-MHz signal is generated in the head and transmitted via planar waveguides to the tines, which constitute a coaxial transmission line. The following parameters are derived from this basic information: temperature corrected ϵ' (real) and ϵ'' (imaginary permittivity), volumetric soil water content, soil salinity, soil conductivity, and temperature-corrected soil conductivity. All sensors were programmed using calibration coefficients based on soil texture and according to the linear relationship between volumetric water content and dielectric permittivity (Topp et al. 1985, Heathman et al. 2003). Additionally, meteorological data (i.e., rainfall, air temperature) were obtained from existing USDA-ARS weather stations in the UCCW network.

Statistical and Temporal Stability Analysis

Exploratory data analysis was first conducted with the measured surface soil moisture data (θ_v) using the mean, standard deviation, box plot, and cumulative frequency plot. In addition, normality of the dataset was tested through Lilliefors test using the *lillietest* function in MATLAB. The Lilliefors test did not reject the null hypothesis that the data are normally distributed at significance level, $P = 0.05$ for most of the observations. Temporal stability was evaluated using the relative difference between individual measurements of soil moisture at location i at time j ($\theta_{i,j}$) and the areal mean soil moisture at the same time ($\bar{\theta}_j$). The relative difference ($\delta_{i,j}$) can be expressed as

$$\delta_{i,j} = \frac{\theta_{i,j} - \bar{\theta}_j}{\bar{\theta}_j} \quad (1)$$

where $\bar{\theta}_j = \frac{1}{N} \sum_{i=1}^N \theta_{i,j}$ and N is the number of sensor

locations. A temporal mean of the relative difference ($\bar{\delta}_i$) and its standard deviation ($\varsigma(\bar{\delta}_i)$) for each location were used to determine the most temporally stable sites according to

$$\bar{\delta}_i = \frac{1}{m} \sum_{j=1}^m \delta_{i,j} \quad (2)$$

and the standard deviation as

$$\varsigma(\bar{\delta}_i) = \sqrt{\frac{\sum_{j=1}^m (\delta_{i,j} - \bar{\delta}_i)^2}{m-1}} \quad (3)$$

where m is the number of measurements at a location.

When temporal mean values are plotted from smallest to largest, one can determine whether a sensor location underestimates or overestimates the field average soil moisture, which has a zero mean relative difference. A smaller standard deviation of a sensor location indicates a greater tendency for that location to be temporally stable.

The nonparametric Spearman's test was also applied to evaluate the temporal stability of different observations. The Spearman's rank correlation coefficient is expressed as

$$r_s = 1 - \frac{6 \sum_{i=1}^n (R_{ij} - R_{ij'})^2}{n(n^2 - 1)} \quad (4)$$

where R_{ij} is the rank of $\theta_{i,j}$ at location i and time j and $R_{ij'}$ the rank of the same variable at the same location but at a different time j' . A Spearman's rank correlation value closer to 1 indicates a stronger tendency of temporal stability between different times.

The root mean square error (RMSE) was determined to further assess offset estimates (Equation 5) at the permanent sensor sites and the most time-stable sites in each field; it was calculated as

$$RMSE = \sqrt{\frac{\sum_{i=1}^N (S_i - O_i)^2}{N}} \quad (5)$$

where N is the number of measured and estimated soil moisture and O and S are the observed and estimated data, respectively. The closer the RMSE value is to 0, the less error in the offset estimate.

Results

In this section we present the experimental results from our agricultural field-scale temporal stability analyses and the results obtained at the larger watershed-scale permanent sensor network. Brief discussions will include the 5- and 20-cm soil moisture data analyses and the possibility of using an offset approach in adjusting the 5-cm permanent sensor data to better represent field-scale average conditions (for field AS1 only).

In Figure 2A, the ranked mean relative differences (MRD) for 5-cm temporary and permanent (P) sensor locations in field AS1 indicate that site 9 is the most temporally stable (smallest standard deviation, ± 0.025) and is close to the field average moisture content (mean offset = $0.059 \text{ m}^3/\text{m}^3$). However, results for the edge-of-field permanent sensor location in Figure 2A show the data to be temporally unstable and to underestimate the field mean by nearly 30 percent. Figure 2B is a plot of the 20-cm sensor results that show site 1 as being temporally stable and the permanent site being unstable and more than 20 percent below the field average soil moisture conditions during the study period. It is important to note that none of the sites at each depth maintain the same ranking in Figures 2A and B. The results for field AS2 (not shown) were very similar to the results for field AS1, although permanent sensor results were closer to field average.

Cumulative frequency (CF) plots for 5- and 20-cm soil moisture data are presented in Figures 3A and B,

respectively, for field AS1. The CF plots allow one to determine if a given location maintains its rank across the study period while identifying sites that represent the watershed average (CF = 0.5). General observation of the plots indicates that the permanent site maintains a low rank and significantly underestimates the field average moisture content at both depths. Also apparent in the graphs are the different ranges in moisture conditions between the two depths, with the range being greatest at the 5-cm depth from $0.15\text{--}0.40 \text{ m}^3/\text{m}^3$.

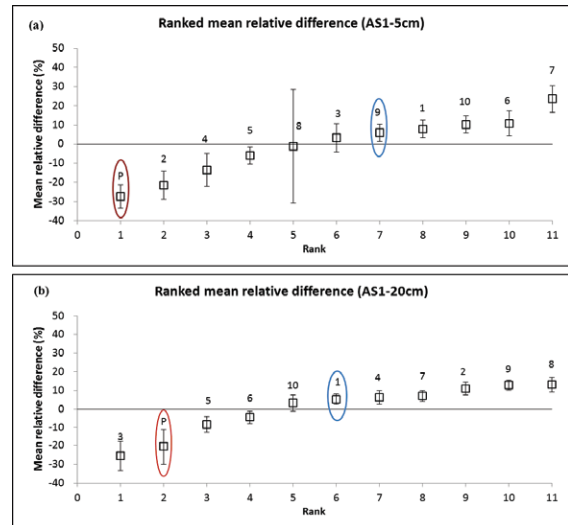


Figure 2. Field AS1 ranked mean relative differences at (A) 5-cm depth, and (B) 20-cm depth.

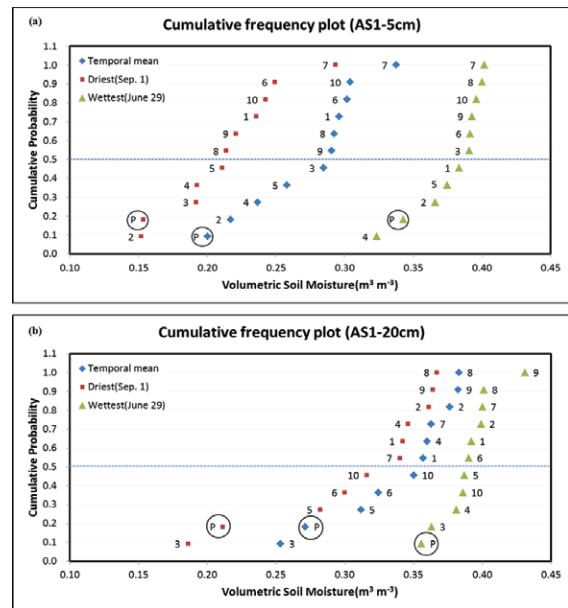


Figure 3. Field AS1 cumulative frequency plots at (A) 5-cm depth, and (B) 20-cm depth.

Grayson and Western (1998) noted that time-stable sites having a nonzero $\bar{\delta}_i$ could be used to represent the field or watershed average θ provided that the offset between the mean values and the nonzero time-stable sites was known. To demonstrate this, Figures 4A and B show linear regression of the estimates based on the work of Grayson and Western (1998). Accordingly, both sites in AS1 give acceptable offset estimates; however, temporary site 9 has the highest R^2 coefficient and the smallest offset and standard deviation.

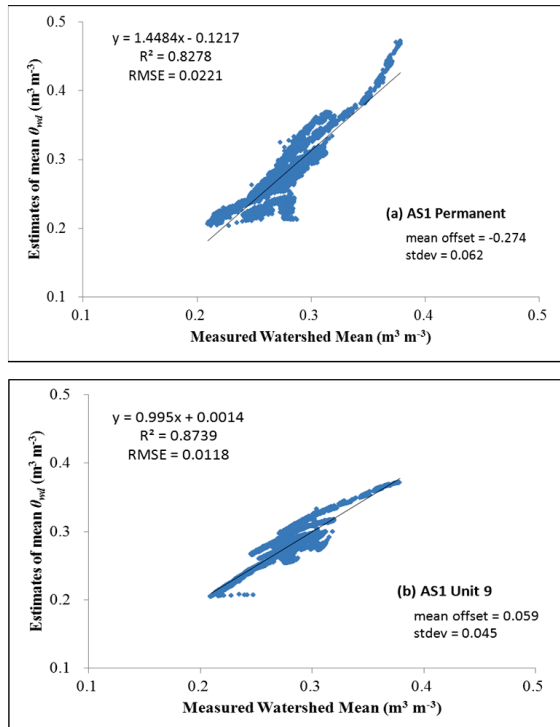


Figure 4. Offset estimates for 5-cm soil moisture in field AS1 for (A) permanent sensor and (B) site 9 locations.

The previous results provide field-scale temporal stability analyses at two sites within the UCCW environmental monitoring network. The final part of this section will show results for all seven permanent soil moisture sites during the study period, covering an area of approximately 6,200 ha, including the two field sites.

The ranked mean relative differences for UCCW soil moisture 5- and 20-cm sensors are given in Figures 5A and B, respectively. Interestingly, the AS1 field site is shown as the most temporally stable site and has an average value very close to the watershed (MRD nearest 0.0 percent). However, results differ at the 20-cm depth with site AME being the most time-stable.

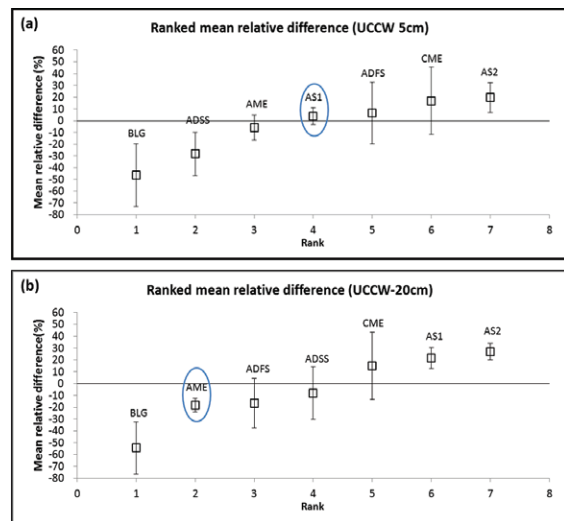


Figure 5. UCCW ranked mean relative differences at (A) 5-cm depth, and (B) 20-cm depth.

The cumulative frequency plots in Figures 6A and B indicate that the range in soil moisture is similar for both depths and that, for a particular site, rank depends on θ conditions at either depth. Sites representative of the watershed mean θ differ depending on depth and θ conditions. Thus, it is important to have θ values ranging from dry to wet conditions to avoid bias.

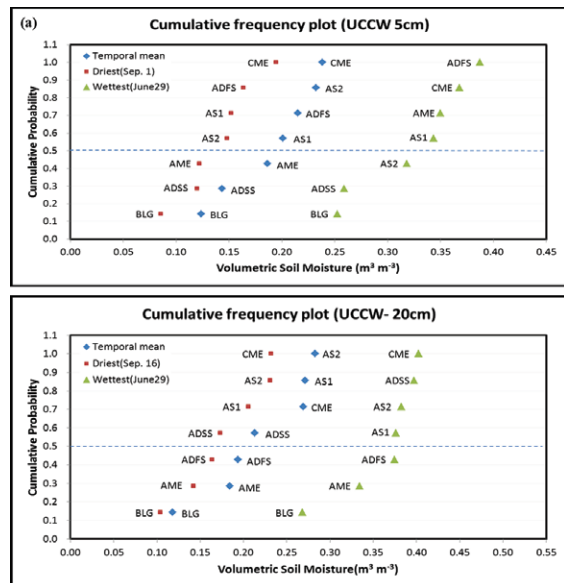


Figure 6. UCCW cumulative frequency plots at (A) 5-cm depth, and (B) 20-cm depth.

Figure 7 illustrates the linear regression for estimates of the watershed mean, again, based on the work of Grayson and Western (1998). For the time period of study, site AS1 appears acceptable as a good representative for estimating the 3- to 9-km-scale

watershed mean (see Figure 1 for scale), which is important considering that the SMAP Cal/Val will consist of data at 3-, 9-, and 36-km resolutions.

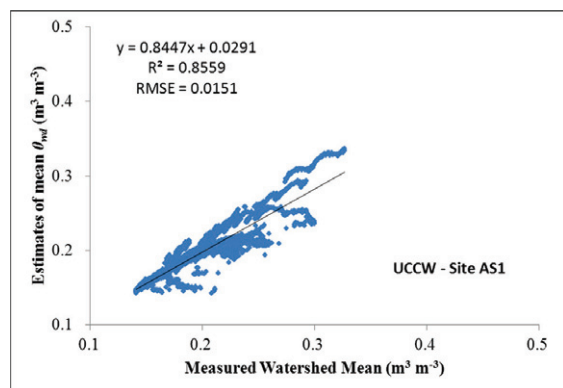


Figure 7. Offset estimates for 5-cm soil moisture for field AS1 in the UCCW soil moisture network.

Conclusions

Temporal stability analyses (TSA) of soil moisture were conducted in an effort to improve the use and representation of permanent in situ sensor data at multiple scales within the Upper Cedar Creek watershed (UCCW) in northeastern Indiana. In general, results indicate that the analyses are sensitive to the scale of observational data (2.5 to 6,200 ha). Spatiotemporal analysis revealed persistent patterns in surface soil moisture and identified sites that were temporally stable at both study scales. However, soil water patterns differed between preferred states (wet/dry) and were primarily controlled by lateral and vertical fluxes. At the field scale, locations that were optimal for estimating the area average water contents were different from permanent sensor locations. However, minimum offset values could be applied to the permanent sensor data to obtain representative field average values of surface θ_v . A TSA of 20-cm θ_v showed little correlation with surface θ_v . TSA results in terms of comparable stable sites at either scale. Recommendations include additional installations of temporary sensors during remote sensing campaigns or special field projects, as well as investigating new approaches for geospatial data analysis in regards to upscaling or downscaling of soil moisture information and interpolation schemes.

Acknowledgments

The authors appreciate the reviews of Chi-hua Huang and Stan Livingston.

References

- Cosh, M.H., T.J. Jackson, R. Bindlish, and J.H. Prueger. 2004. Watershed scale temporal and spatial stability of soil moisture and its role in validating satellite estimates. *Remote Sensing of Environment* 92(4):427–435.
- Cosh, M.H., T.J. Jackson, P. Starks, and G.C. Heathman. 2006. Temporal stability of surface soil moisture in the Little Washita River watershed and its applications in satellite soil moisture product validation. *Journal of Hydrology* 323:168–177.
- Crow, W.T., D. Ryu, and J.S. Famiglietti. 2005. Upscaling of field-scale soil moisture measurements using distributed land surface modeling. *Remote Sensing of Environment* 28:1–14.
- Grayson, R.B., and A.W. Western. 1998. Towards a real estimation of soil water content from point measurements: Time and space stability of mean response. *Journal of Hydrology* 207:68–82.
- Heathman, G.C., P.J. Starks, and M.A. Brown. 2003. Time domain reflectometry field calibration in the Little Washita River Experimental Watershed. *Soil Science Society of America Journal* 67:52–61.
- Njoku, E.G., W.J. Wilson, S.H. Yueh, S.J. Dinardo, F.K. Li, T.J. Jackson, V. Lakshmi, and J. Bolten. 2002. Observations of soil moisture using a passive and active low-frequency microwave airborne sensor during SGP99. *IEEE Transactions on Geoscience and Remote Sensing* 40(12):2659–2673.
- Starks, P.J., G.C. Heathman, L.R. Ahuja, and L. Ma. 2003. Use of limited soil property data and modeling to estimate root zone soil water content. *Journal of Hydrology* 272:131–147.
- Topp, G.C., and J.L. Davis. 1985. Measurements of soil water content performance using time domain reflectometry (TDR): A field evaluation. *Soil Science Society America Journal* 49:19–24.
- Vachaud, G., A. Passerat de Silans, P. Balabanis, and M. Vauclin. 1985. Temporal stability of spatially measured soil water probability density function. *Soil Science Society of America Journal* 49:822–828.